



Resolving abrupt frontal gradients in zooplankton community composition and marine snow fields with an autonomous *Zooglider*

Sven Gastauer , ^{1,2*} Mark D. Ohman ¹

¹Integrative Oceanography Division, Scripps Institution of Oceanography, La Jolla, California, USA

²Thünen Institute of Sea Fisheries, Bremerhaven, Germany

Abstract

An autonomous *Zooglider* navigated across the California Current Front into low salinity, minty waters characteristic of the California Current proper in both summers of 2019 and 2021. Diving to 400 m depth, *Zooglider* transited another near-surface frontal gradient somewhat inshore. These frontal gradients were generally associated with changes in intensity, size composition, and Diel Vertical Migration responses of acoustic backscatterers. They were also associated with pronounced changes in zooplankton community composition, as assessed by a shadowgraph imaging Zoocam. Zoocam detected a decline in concentrations of copepods, appendicularians, and marine snow in the offshore direction, and an overall shift in community structure to a higher proportion of carnivorous taxa (and, in 2019, of planktonic rhizaria). No taxon was consistently elevated at all the peak frontal gradients, but appendicularians, copepods, and rhizarians sometimes showed front-related increases in concentration. Such frontal gradient regions represent relatively abrupt transitions to different communities of planktonic organisms and suspended marine snow particles, with consequences for predator–prey relationships and the dominant vectors of particle export into subsurface waters.

The biophysical properties of frontal gradients in the ocean have attracted increasing interest (e.g., Belkin 2021; Prants 2022), in part as advances in subsurface profiling instruments and autonomous vehicles have made it possible to resolve and revisit such structures. Satellite remote sensing has proven useful for identifying surface and near-surface ocean gradients (e.g., Belkin et al. 2009; Kahru et al. 2018; Haëck et al. 2023) but does not detect subsurface structures. Moreover, measuring changes in physical ocean properties associated with ocean fronts expressed beneath the sea surface has generally proceeded more rapidly than resolving biotic gradients. It is not always clear whether, on smaller scales, organismal abundances and

community structure change in parallel with changes in physical features. Most zooplankton sampling, for example, averages over substantial vertical distances and, in the case of towed nets, over relatively large horizontal scales. The sampling methods can thus obscure the very gradients that are the subject of inquiry.

Some empirical evidence suggests that frontal regions can, under certain circumstances, be sites of higher nutrient fluxes (Li et al. 2017), elevated prey concentration (Powell and Ohman 2015a; Schmid et al. 2020), enhanced grazing activity (Stukel et al. 2017), attraction of mobile predators (e.g., Schmid et al. 2020; Keates et al. 2022), or enhanced vertical export of carbon and other elements (Stukel et al. 2017). Mangolte et al.'s (2023) analysis of biotic gradients across 10 fronts in the California Current Ecosystem distinguished “peak” fronts, where abundance or biomass of planktonic organisms is elevated from “transition” fronts, where gradients occur without biomass enhancement. Numerical models that resolve (sub) mesoscale processes suggest that fine-scale frontal circulation can lead to local enhancement of plankton diversity (Lévy et al. 2018; Mangolte et al. 2022). Lévy et al. (2018) distinguished three types of fronts with different circulation and biotic consequences: (1) passive fronts, where local circulation causes organisms and plankton biomass to stir and mix; (2) active fronts, where enhanced nutrient fluxes stimulate local growth; and (3) reactive fronts, where biotic interactions between organisms lead to local increases in predators and/or

*Correspondence: sgastauer@ucsd.edu; sven.gastauer@thuenen.de

Additional Supporting Information may be found in the online version of this article.

This is an open access article under the terms of the [Creative Commons Attribution](https://creativecommons.org/licenses/by/4.0/) License, which permits use, distribution and reproduction in any medium, provided the original work is properly cited.

Author Contribution Statement: SG and MDO have been involved in the conceptualization, planning, data collection, analysis, writing of initial draft, and revision of the manuscript.

Special Issue: Autonomous Instrumentation and Big Data: New Windows, Knowledge, and Breakthroughs in the Aquatic Sciences. Edited by: Yui Takeshita, Heidi Sosik, Dominique Lefevre, Werner Eckert, Kevin C. Rose, and Deputy Editors Julia C. Mullarney, Steeve Comeau, and Elisa Schaum

prey. However, in general, empirical evidence has lagged behind model predictions.

Apart from in situ bio-optical sensors that are well suited to measuring properties of the ocean environment such as fluorescence, absorption, and scattering of different dissolved and particulate constituents (e.g., Mignot et al. 2018), and targeted DNA sensors (Yamahara et al. 2019), few instruments are available for resolving smaller scale horizontal changes in subsurface ocean plankton communities. This is particularly true for measurements of multicellular organisms, whose aggregation potential at frontal gradients can have important benefits for mobile predators that can exploit locally elevated concentrations of prey (e.g., Schmid et al. 2020).

Optical imaging provides an alternative to net (and pump) sampling of zooplankton, conferring the ability to resolve organisms and marine snow in situ with considerable resolution of microscale habitats in the vertical plane (e.g., Davis et al. 1992; Luo et al. 2014; Briseño-Avena et al. 2020). While conferring enhanced vertical resolution, most imaging approaches to date have been associated with instruments that are lowered from ships or other surface platforms, and are generally deployed at relatively coarse resolution in the horizontal dimension. Horizontally towed shipboard profilers alias fine-scale features. Deployment of in situ imaging devices on fully autonomous and navigable robotic platforms like gliders (e.g., Ohman et al. 2018; Picheral et al. 2022) confers the ability to attain unattended high vertical resolution profiles with suitable horizontal spatial resolution to address questions about the ecological and biogeochemical consequences of (sub)mesoscale horizontal ocean features.

While diverse types of echosounders have been used to characterize bulk properties of acoustic backscattering (e.g., Wiebe and Benfield 2003, De Robertis et al. 2010; Korneliussen 2018), bioacoustic approaches generally lack validation of the identities and characteristics of the backscattering organisms. In addition, conventional echosounders are limited to the larger-bodied organisms that can be resolved at low or medium sound frequencies (typically 10–450 kHz). Acoustic resolution of the smaller-bodied, weakly scattering components of the mesozooplankton community, such as most planktonic copepods, requires high-frequency acoustic transducers (Greenlaw 1979; Stanton et al. 1996). However, due to the rapid absorption of high-frequency sound in seawater (e.g., De Robertis and Higginbottom 2007; Macaulay et al. 2020), it is not feasible to profile large sectors of the water column with high-frequency echosounders deployed from surface vessels or platforms, or from the seafloor. In such deployments, acoustic backscatter can be measured only in very close range from the transducer. To profile through the water column with high frequency sound it is necessary for the acoustic transducer itself to move throughout the water column (Fernandes et al. 2003). While such profiling can be accomplished via a cabled device lowered from the sea surface or raised from the sea floor, tethering can result in

transmission of vibrations and surface wave motion, thereby disturbing the water column and potentially inducing avoidance responses by the target organisms. Deployment of a high frequency transducer on an autonomous glider confers the ability to conduct continuous profiling throughout the entire water column, with equal sampling effort at all depths transited by the glider and with minimal hydrodynamic disturbance of the water column. Furthermore, the combination of a high frequency (e.g., 1000 kHz) with a medium frequency (e.g., 200 kHz) transducer on a glider makes it possible to assess both smaller and larger sources of backscatter and to approximate the size spectrum of the acoustic scattering community (e.g., Gastauer et al. 2022).

The California Current System is a complex of currents including the southward flowing California Current in offshore waters, the Inshore Countercurrent in proximity to the coast, and the California Undercurrent in subsurface waters (Hickey 1979; Lynn and Simpson 1987). Surface waters are advected offshore, especially during the upwelling season (Chavez et al. 1991, Chabert et al. 2021), often associated with upwelling filaments (Chabert et al. 2021) and mesoscale eddies (Chelton et al. 2007). Despite this complexity, there is typically a horizontal gradient where colder, higher salinity, lower dissolved oxygen waters found close to the coast meet southward-flowing California Current water somewhat offshore (Lynn and Simpson 1987). The California Current proper is distinguished by a low salinity core, which is expressed in near-surface or subsurface waters (Lynn and Simpson 1987), arising from its origins in the Subarctic North Pacific. Hence, there is a somewhat predictable gradient between the higher salinity near-shore waters and the lower salinity offshore California Current waters, although the offshore extent of the frontal boundary region between the two is highly variable.

Here we address the following questions regarding the major frontal gradients that are often encountered when transiting from the nearshore coastal ocean to the offshore California Current using data from a 2-week *Zooglider* mission conducted in 2019 and in 2021:

Do zooplankton community structure and body size change at major frontal gradients across the California Current System?

If so, which taxonomic and functional groups are most affected?

Does Diel Vertical Migration behavior change across such frontal gradients?

Are frontal regions sites of elevated biomass of phytoplankton, marine snow, or mesozooplankton?

Materials and methods

Zooglider was deployed during the California Current Ecosystem—Long Term Ecological Research (CCE-LTER) process cruises in 2019 (August 13–27) and 2021 (July 21 to August 9) from the R/V *Atlantis* and R/V *Roger Revelle*,

respectively, 15.7 and 19.4 km offshore of Point Sur, California, USA, in the 2 yr (Figure Supporting Fig. S1). Full *Zooglider* engineering details are described in Ohman et al. (2018). *Zooglider* followed a programmed route in an offshore direction (westwards), which was updated daily via two-way Iridium communication. Generally, *Zooglider* dove to 400 m, completing a dive approximately every 3 h, recording data only during each dive ascent. Ascent and descent angles were $\sim 17^\circ$ and vertical velocities $\sim 0.1 \text{ m s}^{-1}$. To sense the physical environment surrounding *Zooglider*, a pumped conductivity, temperature, and depth unit (CTD, SeaBird CP41), and a chlorophyll *a* (Chl *a*) fluorometer (Seapoint mini-scf), are used. Fluorometers were calibrated regularly using standardized dilutions of pure Chl *a* (Sigma Life Sciences) dissolved in 90% acetone as described by Powell and Ohman (2015a). Each calibration provided a slope value ($\text{mg Chl } a \text{ L}^{-1} \text{ V}^{-1}$) allowing the translation of measured fluorescence counts into concentrations of Chl *a* expressed in standardized fluorescence units (SFU; Powell and Ohman 2015a). Spiciness was derived from salinity and temperature measurements, following McDougall and Krzysik (2015). Spicier water corresponds to warmer, saltier water while colder, fresher water is considered minty. Gradients of hydrographic conditions were based on the rolling average of 5 m of depth by three dives. Fronts were defined by locations of maximum salinity and spice gradients in the upper 50–100 m (Supporting Information Figs. S2, S3). Ocean turbidity was approximated by the attenuation coefficient of light at 490 nm (m^{-1} ; K_{d490} , courtesy of M. Kahru, Scripps Institution of Oceanography). Higher K_{d490} values correspond to a shallower attenuation depth, hence more turbid water. K_{d490} values were extracted at dive locations from the ESA Ocean Color Climate Change Initiative (v.3.0), global level 3 binned multisensor time series of satellite ocean color data with 4 km resolution. For each geographical location, the temporally closest daily value was used (i.e., if no value for a given day was available, the temporal search radius was extended by 1 d until a value was found).

Optical data acquisition and processing

The imaging system on *Zooglider* is a custom optical shadowgraph (Zoocam) with telecentric lens, red light illumination, and a sampling volume of 250 mL (Ohman et al. 2018; Ellen et al. 2019). Optical images are acquired at a sampling rate of 1 or 2 Hz during the glider's ascent, providing maximal vertical sampling resolution of 5–10 cm. Raw optical images acquired by Zoocam are processed post mission. Sequential flatfield correction and segmentation of individual regions of interest (ROIs) are applied, followed by classification using deep learning methods, after Ellen et al. (2019). Occasionally, stuck tentacles interfered with image acquisition and such frames were removed from further analysis. Small particles 0.25–0.45 mm in equivalent circular diameter (ECD) are recorded with summary metrics but are not classified. These small particles have been found to be composed mainly of

marine snow (Ohman et al. 2018; Briseño-Avena et al. 2020; Fakhraee et al. 2020; Whitmore and Ohman 2021). Particles $\geq 0.45 \text{ mm ECD}$ are recorded, measured, and attributed to a taxonomic class following machine learning algorithms with finely tuned hyperparameters that also incorporate context metadata (Ellen et al. 2019). Our current model distinguishes 58 taxonomic classes with an average *F1* score (predictive power derived from the precision and recall metrics) of 94.9% (Supporting Information Fig. S4). Here, we focus on nine dominant groups of organisms and particles: appendicularians, chaetognaths, copepods—*Oithona*-like (hereafter “*Oithona*”), copepods-other (comprised mainly of calanoid copepods), doliolids + salps (plus rarely small pyrosomes), euphausiids (which occasionally includes a decapod shrimp), gelatinous predators (medusae, siphonophores, and ctenophores), rhizarians (Acantharia, Collodaria, Phaeodarea, and Foraminifera), and marine snow. Taxon-specific precision and recall for our Machine Learning model can be seen in Supporting Information Fig. S4. Although fast-swimming organisms could potentially avoid the glider and introduce a bias toward smaller, slower swimming specimens, Whitmore and Ohman (2021) demonstrated that taxonomic composition, and size distributions derived from Zoocam are comparable to those obtained from MOCNESS samples, including fast-swimming organisms such as euphausiids.

Feret diameter (mm, i.e., the maximum dimension across a ROI) was used as a proxy for the master trait of body size from optical images. Following size class definitions from Gastauer et al. (2022) for acoustic backscatter, three mesozooplankton size categories were defined: large ($> 3 \text{ mm}$), intermediate (1–3 mm), and small ($< 1 \text{ mm}$). The community functional composition was split into picograzers (appendicularians, doliolids, and salps), omnivores (all copepods and euphausiids), and carnivores (chaetognaths and gelatinous predators). Carbon biomass was determined from updated equations from Lavaniegos and Ohman (2007) relating taxon-specific body size (here as Feret diameter) to organic carbon content (Supporting Information Table S2).

We tested for spatial differences in abundance of each major taxon on two scales across the *Zooglider* track. First, we analyze the regional cross-shore scale, using the Kruskal–Wallis test with Dunn pairwise post hoc test. Here, we compare abundances among three regions: inshore, midshore (region between the two fronts), and offshore. Then, we test for changes in abundance on the local front scale, using the Mann–Whitney *U* test. Here, we compare abundances at the front compared with concentrations measured at *Zooglider* dives immediately before and after the front. A sequence of six dives was selected for one day-night sequence immediately preceding and one sequence immediately following the day-night sequence associated with the hydrographically defined frontal region.

Acoustic data acquisition and processing

Zooglider is equipped with a custom active acoustic system, Zonar, consisting of single-beam 200-kHz (3 dB beam angle $\theta_{3 \text{ dB } 200 \text{ kHz}} = 9.8^\circ$) and 1000-kHz ($\theta_{3 \text{ dB } 1000 \text{ kHz}} = 4^\circ$) transducers

manufactured by the Instrument Development Group at the Scripps Institution of Oceanography. Every 4 m of depth during the glider ascent, a four-ping burst ensemble was emitted sequentially at each of the two frequencies (four pings at 200 kHz, followed by four pings at 1000 kHz). The inter-ping interval was 200 ms (ping rate = 5 Hz) for the 200 kHz and 100 ms (ping rate = 10 Hz) for the 1000 kHz. A 1-ms blanking time for both, which extends further than the theoretical nearfield zone of the transducers, was applied. For the present study, only data within a range of 3–6 m from the transducer face were considered. Ambient sound speed and absorption coefficients were computed directly from the *Zooglider* temperature, salinity, and pressure values following Mackenzie (1981) and Francois and Garrison (1982a,b). Details on the acoustic data processing may be found in Gastauer et al. (2022). Zonar calibration largely followed procedures for single-beam transducers in Demer et al. (2015), using a 10-mm tungsten carbide sphere with cobalt binding. Calibrations were completed on a regular basis in a purpose-built pool at the Scripps Institution of Oceanography. Acoustic density information was partitioned into size-stratified classes based on the scattering properties of dominating organisms, using dB differencing at the two available frequencies, following methods described in Gastauer et al. (2022).

Results

Hydrographic conditions

The 2019 and 2021 *Zooglider* missions off Pt. Sur covered geographically similar domains (Supporting Information Fig. S1). There is considerable hydrographic variability across the region, on multiple spatial scales (Fig. 1; Supporting Information Fig. S1; Table S1). In both years, surface temperatures increased strongly westward (i.e., offshore, Spearman's rank correlation between longitude and temperature, $p < 0.001$ for both years) (Supporting Information Figs. S1, S2; Table S1). In the present study, we focus on the strongest frontal gradients resolved along the *Zooglider* trajectories. In both years, two main fronts were identified, one “inshore” front (ca. 100 km [in 2019] to 130 km [in 2021] along track from the beginning of the *Zooglider* transit) and one “offshore” front (160 km along track in 2019 and 180 km along track in 2021; Fig. 1; Supporting Information Figs. S1–S3). The two fronts were defined as the regions of steepest salinity and spice gradients, while other smaller fronts or filaments were also evident in the observed hydrographic data (Fig. 1; Supporting Information Figs. S2, S3). The presence of the California Current is evidenced by a steep decrease in salinity offshore (Fig. 1; Supporting Information Figs. S2, S3). In 2019, generally lower salinity values were observed (Fig. 1; Supporting Information Fig. S2; Table S1). Analogously, spice increased westward, until the steep decrease of salinity occurred and the water became much mintier (Fig. 1; Supporting Information Fig. S2; Table S1). In both years, the highest Chl *a* fluorescence, as a proxy for Chl *a* concentration, was observed inshore of the

inner front ($p < 0.05$; Fig. 1), displaced somewhat from shore. When front-related values were compared with those at glider dives immediately preceding and following the fronts, there was evidence of elevated Chl *a* fluorescence in the upper 50 m at the inshore front in 2019 ($p < 0.05$), but not at the other frontal locations.

Acoustic backscatter

In both years, overall acoustic backscatter (S_v , dB re 1 m^{-1}) was stronger at 1000 than at 200 kHz, suggesting an overall greater influence of smaller-bodied scatterers ($\Delta_{S_v 1000-200} > 0$ dB; Fig. 2a–d). Average S_v at both 200 and 1000 kHz was highest in the inshore region in both years (Kruskal–Wallis, $p < 0.05$). The size composition of acoustic backscatterers in the upper 100 m did not differ among regions ($p > 0.05$), as indicated by similar values of $\Delta_{S_v 1000-200}$ (Fig. 2e,f). However, deeper than 100 m, there was a marked change in the relative importance of small and larger backscatterers, with smaller backscatterers (reddish shading in Fig. 2e,f) consistently dominating the layer between 100 and 300 m in the offshore region ($p > 0.05$). There was no evidence of front-related increases in S_v at either front in either year (Mann–Whitney U , $p > 0.10$).

Diel vertical migration

Diel vertical migrations were consistently deeper in the offshore, more transparent waters. The average daytime depth occupied by backscatterers at both 200 and 1000 kHz deepened in the offshore direction, with a deepening of daytime depth offshore of both fronts in 2019 and offshore of the inshore front in 2021 ($p < 0.01$; Fig. 2g,h). Satellite-measured light extinction also varied in the offshore direction, with more optically transparent waters (i.e., lower K_{d490}) in the offshore in both years ($p < 0.001$; Fig. 2g,h). Transparency increased just offshore of both fronts in 2019 and just offshore of the inshore front in 2021 (Fig. 2g,h). The daytime depth occupied by 200 kHz acoustic scattering layers was highly (inversely) correlated with light attenuation in the overlying water column ($p < 0.001$) in both years. The daytime depth of the 1000 kHz layer was inversely related to light attenuation in 2019 ($p < 0.001$) but not in 2021 ($p = 0.06$; Supporting Information Table S3). Animals migrated deeper in optically clearer waters. The mean daytime depths at 200 and 1000 kHz did not differ significantly in 2019 (Wilcoxon signed-rank matched pairs test, $v = 61$, $p > 0.1$) but were somewhat deeper at 200 kHz in 2021 ($v = 104$, $p = 0.01$).

Zooplankton community structure

The imaging Zoocam resolved cross-shore and cross-frontal changes in concentration, vertical distribution, and size composition of the zooplankton community and marine snow. We present the results in an approximate sequence of increasing trophic level, from metazoan picograzers, to omnivores, to carnivores, although this is of course an oversimplification of

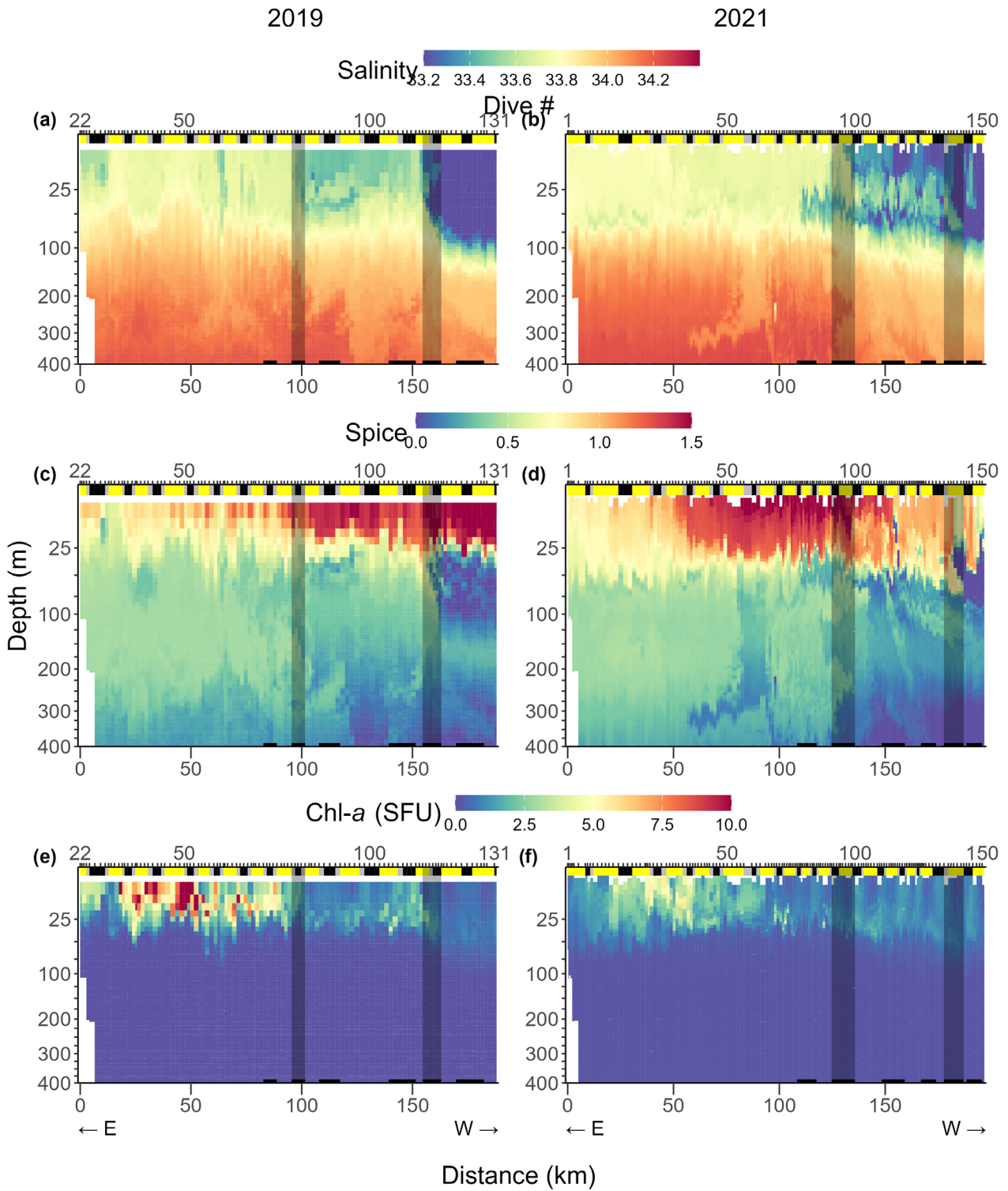


Fig. 1. Zooglider sections across two major frontal regions (vertical gray bars) in (left column) 2019 and (right column) 2021. Top row (a, b): salinity. Middle row (c, d): spiciness. Lower row (e, f): chlorophyll *a* (Chl *a*) fluorescence. Horizontal black bars at the bottom of each figure indicate locations of dives preceding, inside, and following the peak frontal gradients. The top *x*-axis shows Zooglider dive number, with color bar indicating day (yellow), dusk/dawn (gray), or night (black) dives. The bottom *x*-axis indicates distance traveled (km), generally from eastward (nearshore) to westward (offshore). Note that the *z*-axis has been square root-transformed.

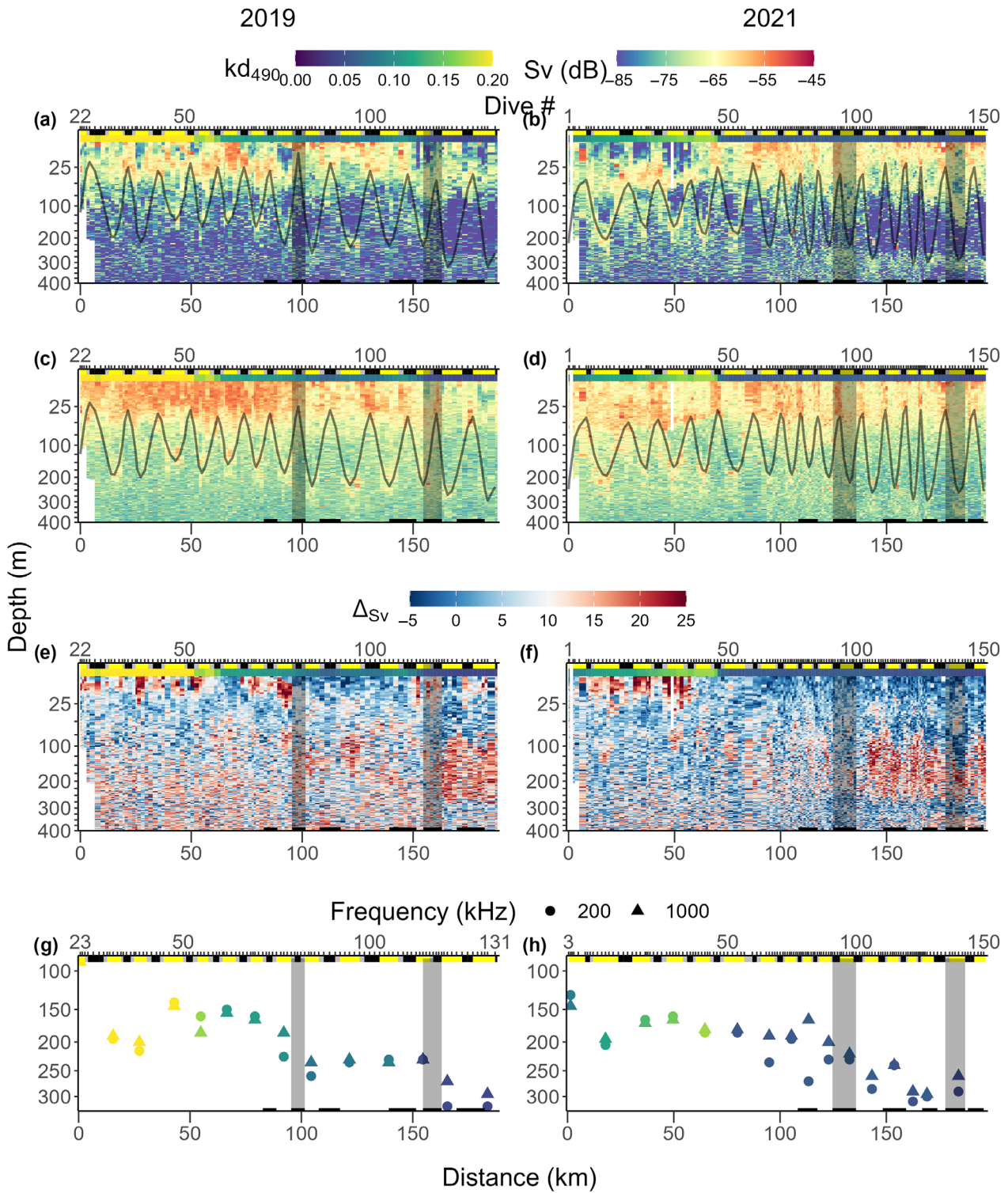


Fig. 2. Zooglider sections of acoustic backscattering volume (Sv) in (left) 2019 and (right) 2021, with: Top row (a, b): Sv at 200 kHz. Second row (c, d): Sv at 1000 kHz. Third row (e, f): $\Delta S_v = S_{V1000\text{ kHz}} - S_{V200\text{ kHz}}$. Fourth row (g, h): Daytime depths of scattering layers at 200 and 1000 kHz, with K_{d490} as symbol color. The top color bar indicates day (yellow), dusk/dawn (gray) or night (black) dives and for the top three rows a second color bar indicates light extinction at 490 nm (K_{d490}). Horizontal black bars at the bottom of each figures indicate locations of dives preceding, inside, and following the peak frontal gradients. Vertical gray bars indicate the locations of the inshore front (left bar in both panels) and offshore front (right bar in both panels). Continuous dark gray lines in first and second rows indicate the day and night depths of the 50th percentile of Sv. Vertical gray bars indicate the locations of the inshore front (left bar in both panels) and offshore front (right bar in both panels). The top x-axis indicates dive number and the bottom x-axis indicates distance traveled (km). Note that the z-axis has been square root transformed.

dietary breadth of each of the taxa considered. We present spatial differences detected for each major taxon on two spatial scales: first, on the regional cross-shore scale and then on the local frontal scale.

Metazoan picograzers included appendicularians, plus a combined assemblage of doliolids and salps. At the regional scale, appendicularians were present in reduced concentrations offshore in both 2019 and 2021 ($p < 0.05$; Fig. 3a–c), with diminished body sizes in the offshore region in 2019 ($p < 0.01$; Fig. 3d–f). On the local frontal scale, appendicularian concentrations were lower at the peak frontal gradient region in the offshore front in 2019 and elevated at the inshore front in 2021 ($p < 0.05$). In notable contrast with the appendicularians, doliolids + salps showed reduced concentrations in the inshore region in both years ($p < 0.001$; Fig. 3g–i), with similar body sizes throughout in 2019 and larger body sizes inshore in 2021 ($p < 0.01$; Fig. 3j–l). This suggests that appendicularian habitats were generally more favorable in the inshore region, while doliolids + salps habitats were generally more favorable in the midshore to offshore region. For the doliolids + salps on the local frontal scale, there was an increase in concentration at the inshore front, but only in 2021 ($p < 0.01$).

Two groups of copepods (copepod-others [which excludes the genus *Oithona*] and *Oithona*-like copepods) exhibited contrasting patterns. Copepod-others showed decreased concentrations in the offshore region in both 2019 and 2021 ($p < 0.001$; Fig. 4a–c), accompanied by a larger average body size in the inshore region ($p < 0.01$; Fig. 4d–f). In contrast, *Oithona* copepods showed lowest concentrations in the inshore in both years ($p < 0.001$; Fig. 4g–i). There was a notable deepening of vertical distributions of *Oithona*-like copepods offshore of the offshore front in 2019 and the inshore front in 2021 (Fig. 4). *Oithona* body sizes were larger in the inshore region ($p < 0.001$; Fig. 4j–l). There was a front-related local increase in concentrations of copepod-others and *Oithona* at the inshore fronts in 2019 and 2021 and an increase in *Oithona* the offshore front in 2019 ($p < 0.05$).

Euphausiid concentrations decreased in the offshore region in 2019 ($p < 0.01$; Fig. 5a–c). Body sizes did not show evidence for change on the regional scale ($p > 0.10$; Fig. 5d–f). There was no evidence for front-related change in euphausiid concentrations ($p > 0.20$) in either year.

Turning to carnivorous metazoans, the gelatinous predators (comprising hydromedusae, ctenophores, and siphonophores) showed decreased concentrations in the inshore region in both years ($p < 0.001$; Fig. 6a–c). Predator body sizes were larger in the inshore region in 2021 ($p < 0.05$; Fig. 6d–f). At the local frontal scale, there was no evidence of front-related changes in concentrations of gelatinous predators in either year ($p > 0.05$). Chaetognaths, which are also obligate predators, showed different spatial patterns in the 2 yr, with decreased concentrations in the offshore region in 2019 and decreased concentrations in the inshore in 2021 ($p < 0.001$; Fig. 6g–i). Chaetognaths were also larger in the inshore than

the offshore region ($p < 0.05$; Fig. 6j–l) in both years. There was no evidence of local front-related change in chaetognath concentrations in either year ($p > 0.20$).

Planktonic Rhizaria (comprising, in decreasing order of numerical importance: Acantharians, Collodarians, Phaeodarians, and Foraminifera) showed taxon-specific changes in the cross-shore direction that are largely masked by the composite sections that sum these taxa together in Fig. 7a–f (see Supporting Information Figs. S5–S8 for taxon-specific changes). Overall, total rhizarian concentrations were elevated in the mid-shore region in 2019 ($p < 0.05$; Fig. 7a–c). Rhizarians were smaller inshore in both years ($p < 0.001$; Fig. 7d–f). The bimodal distribution of cell sizes in the vertical plane in Fig. 7d,e reflects a dominance of acantharians and collodarians in the euphotic zone (0–75 m) and a dominance of larger phaeodarians in waters between 100 and 300 m (cf. Biard and Ohman 2020). At the local scale, total rhizarians were present at higher concentrations at the inshore fronts in both 2019 and 2021 ($p < 0.05$), but not at the offshore fronts.

The concentration of marine snow declined abruptly in the offshore region in both 2019 and 2021 ($p < 0.01$; Fig. 7g–i). The average size of marine snow was somewhat smaller inshore in both years ($p < 0.05$; Fig. 7l). (Note that Fig. 7l averages across all depths.) In general, marine snow tends to occur in much higher concentrations, but smaller sizes in the inshore region. There was little evidence of front-related changes in concentration of marine snow ($p > 0.40$), apart from a local increase at the inshore front in 2021 ($p < 0.001$).

We summarize the cross-shore and cross-frontal changes in overall community structure in three ways in Fig. 8: (a, b) the proportional composition of different taxa; (c, d) the proportional composition of different trophic guilds; and (e, f) the proportional composition of different body sizes. These community summaries, expressed as proportions of C biomass, are based on the upper 100 m where most zooplankton taxa were concentrated. The taxon-based community structure summary reveals a reduced contribution of both copepods and appendicularians and an increased contribution of gelatinous predators in the offshore region in 2019 ($p < 0.01$; Fig. 8a). Changes were most pronounced just offshore of the two frontal regions. Somewhat analogous changes were seen in 2021, where copepods were elevated and gelatinous predators decreased in proportional composition inshore ($p < 0.001$; Fig. 8b). *Oithona* copepods showed a larger proportional contribution in the offshore in 2019 and smaller proportional composition in the inshore in 2021 ($p < 0.001$; Fig. 8a,b). Rhizaria showed a consistently diminished proportional composition in the inshore region in both years ($p < 0.001$; Fig. 8a,b). Doliolids + salps showed a reduced contribution inshore in 2019 ($p < 0.001$), but no significant regional change in proportional composition in 2021 ($p > 0.20$; Fig. 8a,b).

The representation of the community as trophic guilds (Fig. 8c,d) showed reduced contributions of carnivores in the

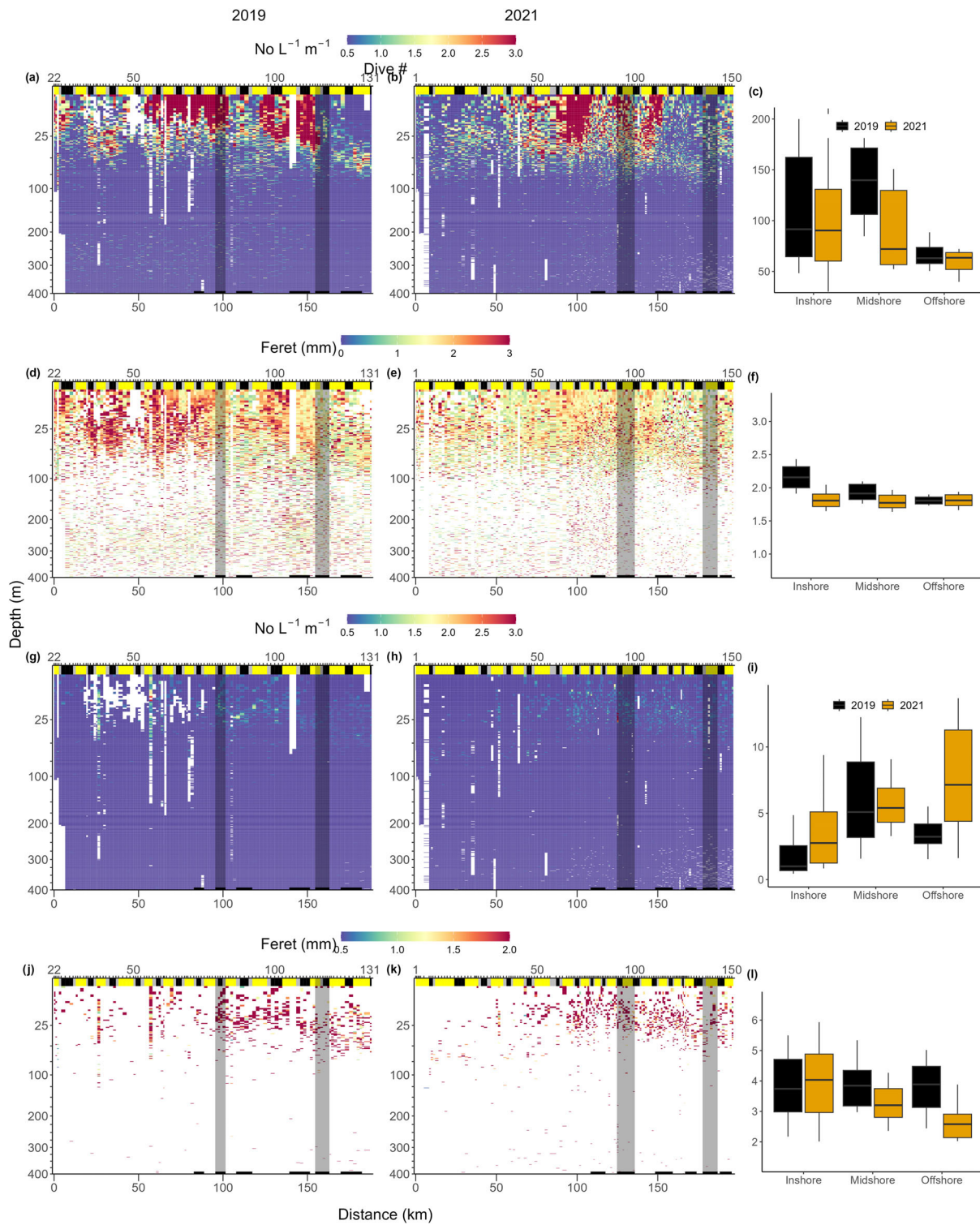


Fig. 3. Upper two rows (a–f): appendicularians and lower two rows (g–l): doliolids + salps, as concentration (a, b, g, h, No. L⁻¹) and size (d, e, j, k, Feret diameter, mm). *Zooglider* deployments in (left columns) 2019 and (center columns) 2021. Top color bar indicates day (yellow), dusk/dawn (gray), or night (black) dives. Horizontal black bars at the bottom of each figures indicate locations of dives preceding, inside, and following the peak frontal gradients. Vertical gray bars indicate the locations of the inshore front (left bar in both panels) and offshore front (right bar in both panels). Top x-axis indicates dive number, bottom x-axis indicates distance traveled (km). Note that the z-axis has been square root-transformed. Boxplots in right columns grouped by year (black = 2019, orange = 2021) and by region inshore of the inner front, midshore between the two fronts, or west of the front. Box plots indicate median \pm 10th and 90th percentiles, depth-integrated for each location.

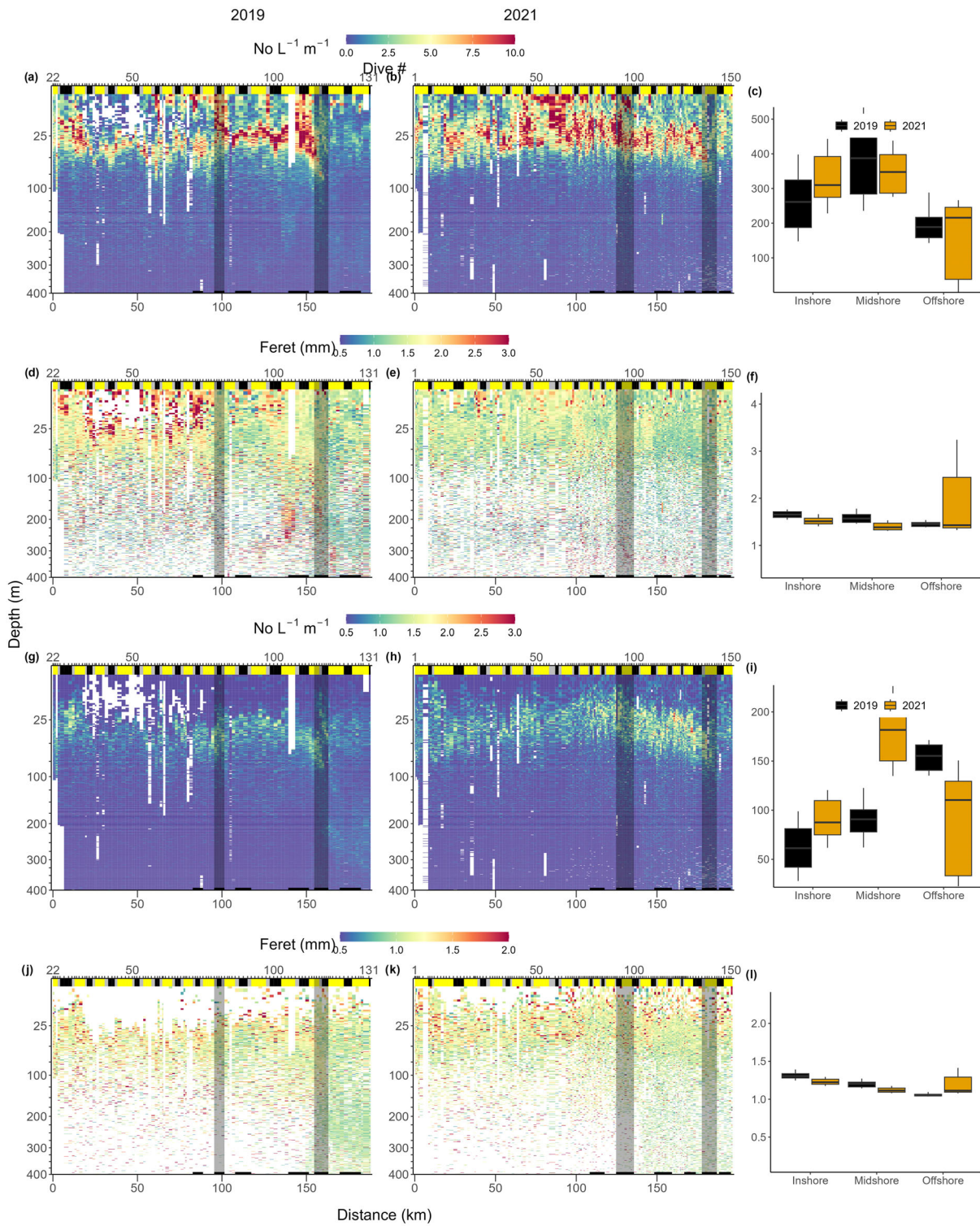


Fig. 4. Upper two rows (a–f): copepods-others and lower two rows (g–l): *Oithona*-like copepods, as concentration (no. L⁻¹) and size (Feret diameter, mm). Other details as in Fig. 3.

inshore region in both years ($p < 0.001$). Summarized in terms of body size (Fig. 8e,f), the smaller-bodied zooplankton showed reduced proportional contributions nearshore ($p < 0.001$).

Overall, both acoustic and optical measures recorded increased representation of smaller-sized organisms in the midshore or offshore region.

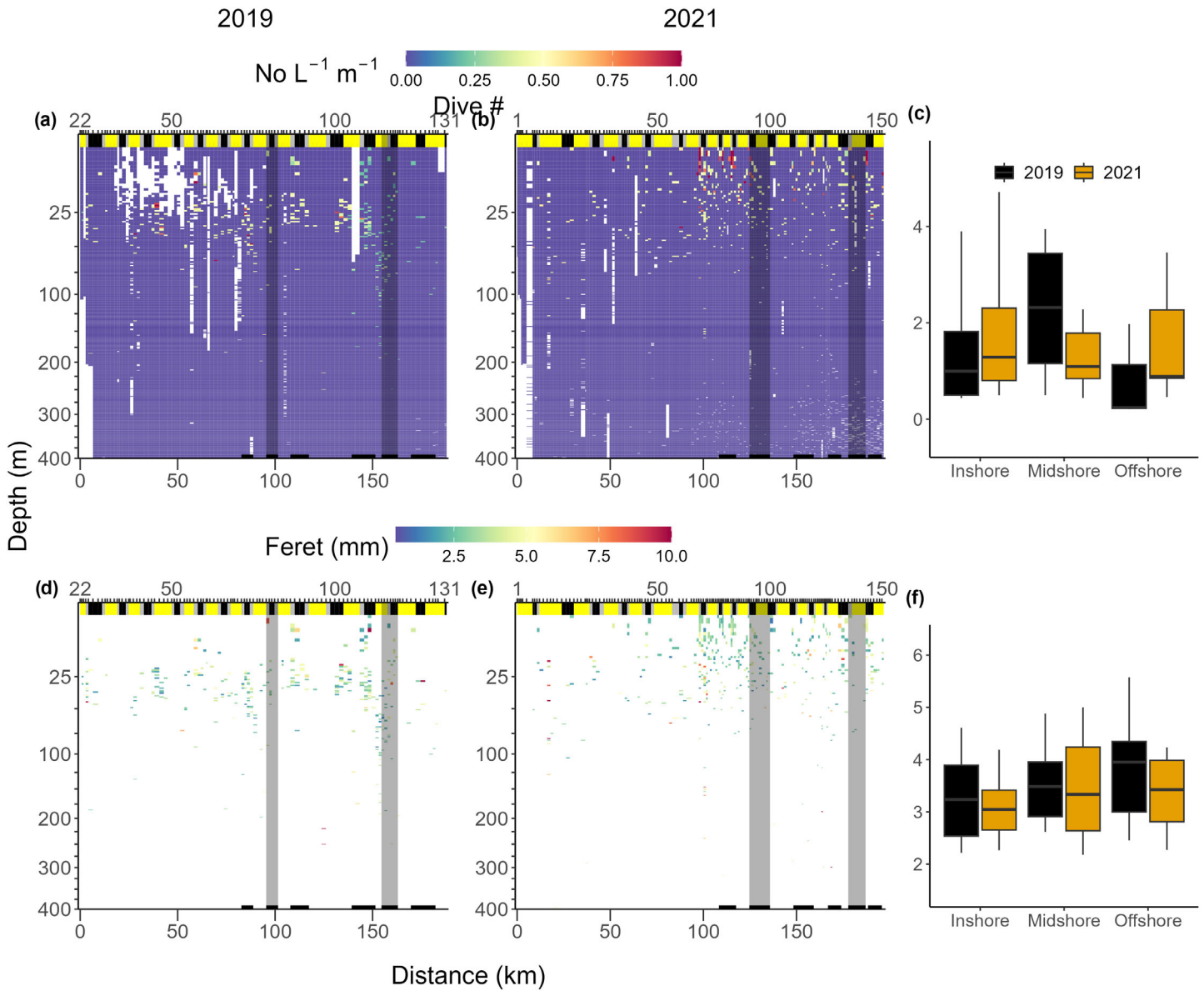


Fig. 5. Upper row (a–c): euphausiids, as concentration (no. L^{-1}) and lower row (d–f): size (Feret diameter, mm). Other details as in Fig. 3.

Discussion

Do zooplankton community structure and body size change at major frontal gradients?

In both study years, *Zooglider* crossed multiple hydrographic features, but most prominently an offshore frontal gradient into low salinity, minty waters characteristic of the California Current proper (cf. Hickey 1979; Lynn and Simpson 1987), which we call the California Current Front. Another significant frontal gradient, also defined by salinity and spiciness, occurred somewhat inshore of the California Current Front. These frontal gradients were generally associated with changes in volume backscatter, size composition, and Diel Vertical Migration responses of acoustic

backscatterers. These gradients were also associated with a pronounced decline in concentrations of copepods and appendicularians, and an overall shift in community structure to increased representation of smaller-bodied organisms and a higher proportion of carnivorous taxa in the offshore. In 2019, a higher proportion of planktonic rhizaria occurred in the offshore direction. Marine snow concentrations also decreased consistently in the offshore direction. Therefore, these frontal gradients can represent relatively abrupt transitions to different communities of planktonic organisms and suspended marine snow particles, with consequences for predator–prey relationships and sources of carbon export.

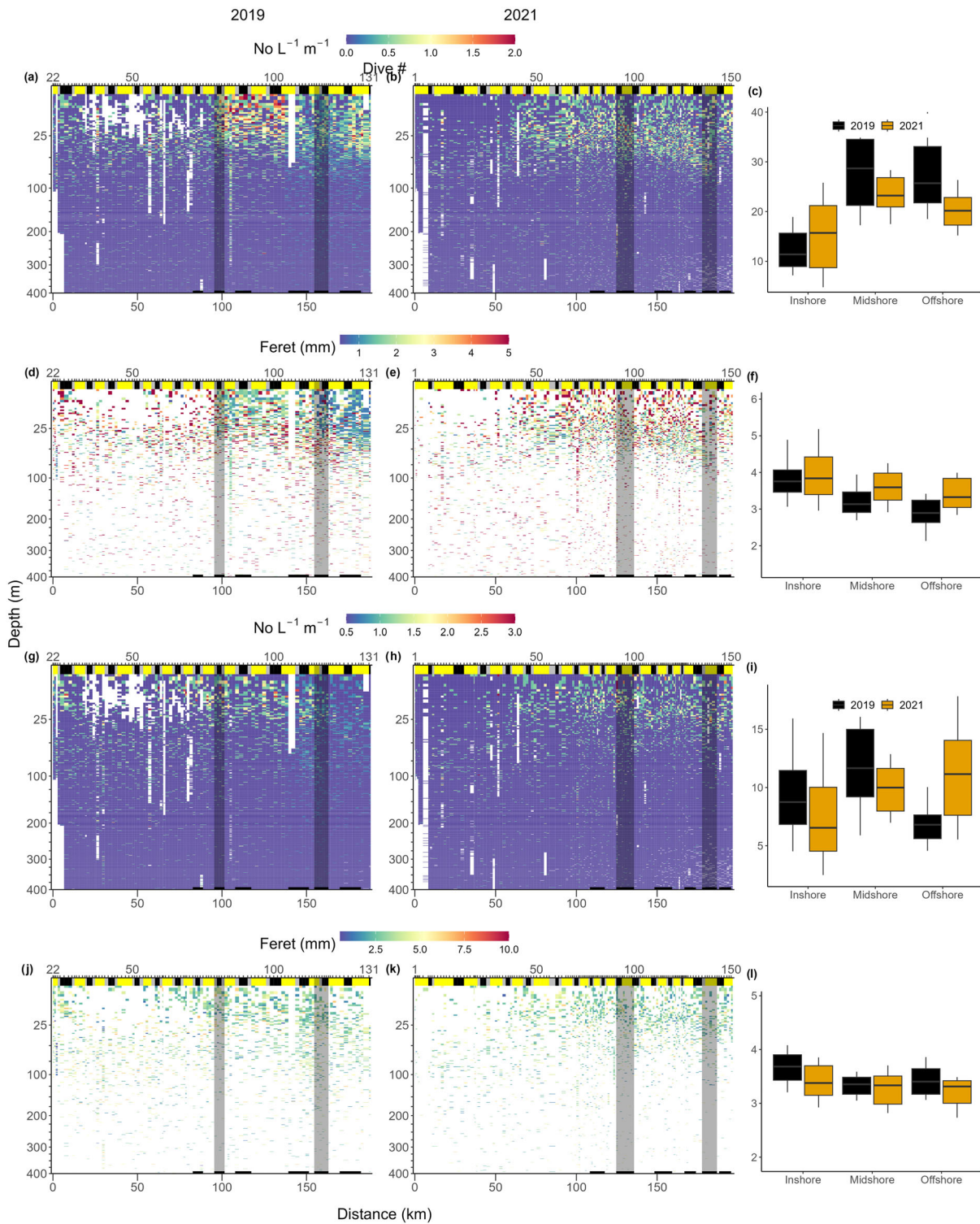


Fig. 6. Upper two rows (a–f): gelatinous predators and lower two rows (g–l): chaetognaths, as concentration (no. L⁻¹) and size (Feret diameter, mm). Other details as in Fig. 3.

Which taxonomic and functional groups are most affected?

There were distinct differences among pelagic tunicates, with marked declines in concentrations of appendicularians

offshore, but reductions in concentrations of doliolids + salps inshore of the major frontal features. Here, we treat all detected appendicularians, doliolids + salps as potential picoplankton grazers. This is a simplification, and we expect differences within

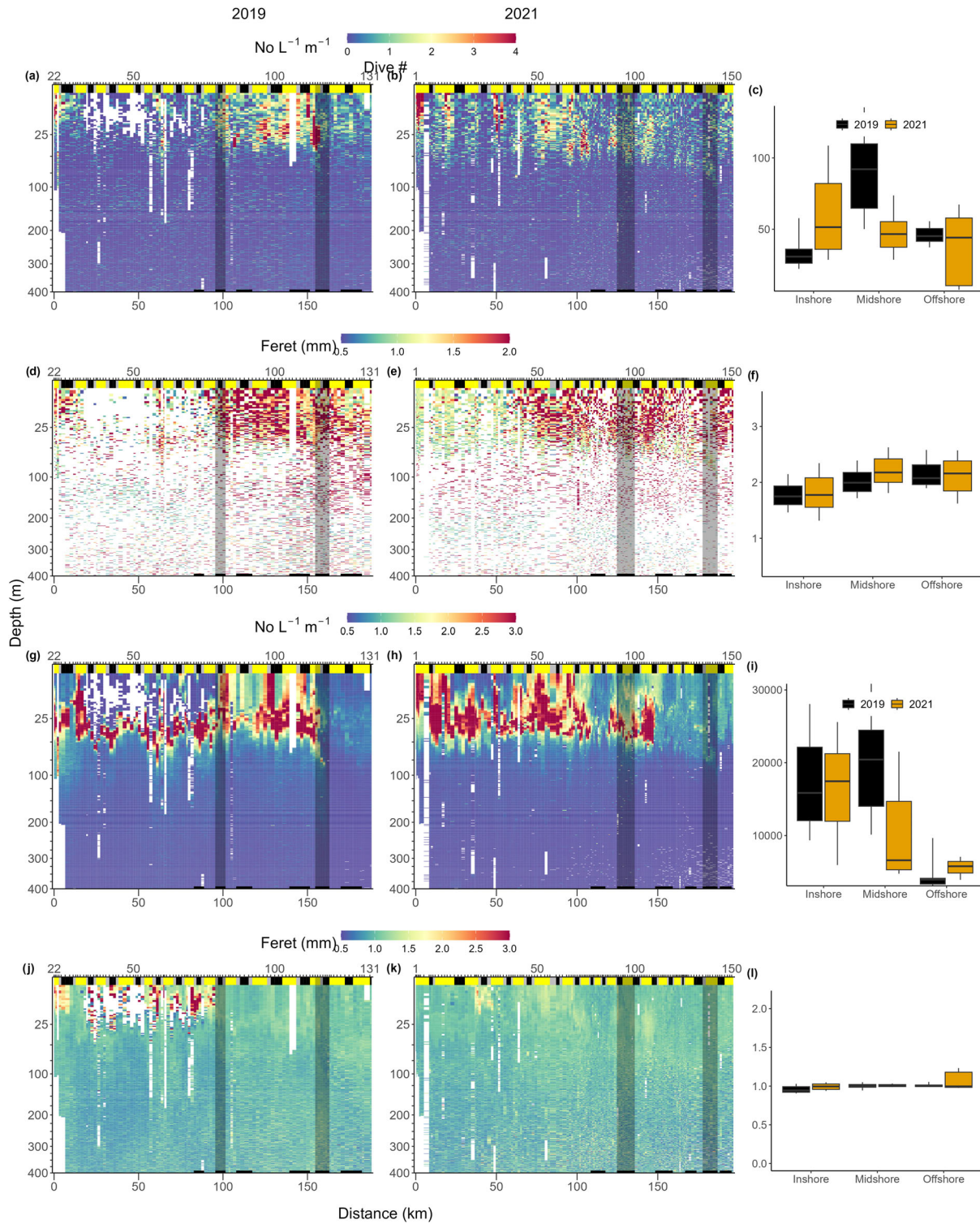


Fig. 7. Upper two rows (a–f): rhizarians and lower two rows (g–l): marine snow, as concentration (no. L⁻¹) and size (Feret diameter, mm). Other details as in Fig. 3.

these taxa in terms of prey preferences, susceptibility to predators, and habitats occupied (e.g., Bone 1998; Deibel 1998a,b; Sutherland et al. 2010; Dadon-Pilosof et al. 2019; Decima

et al. 2019). The important role that abandoned appendicularian houses can play in vertical export of C and other elements (Allredge 1972; Robison et al. 2005) suggests that the

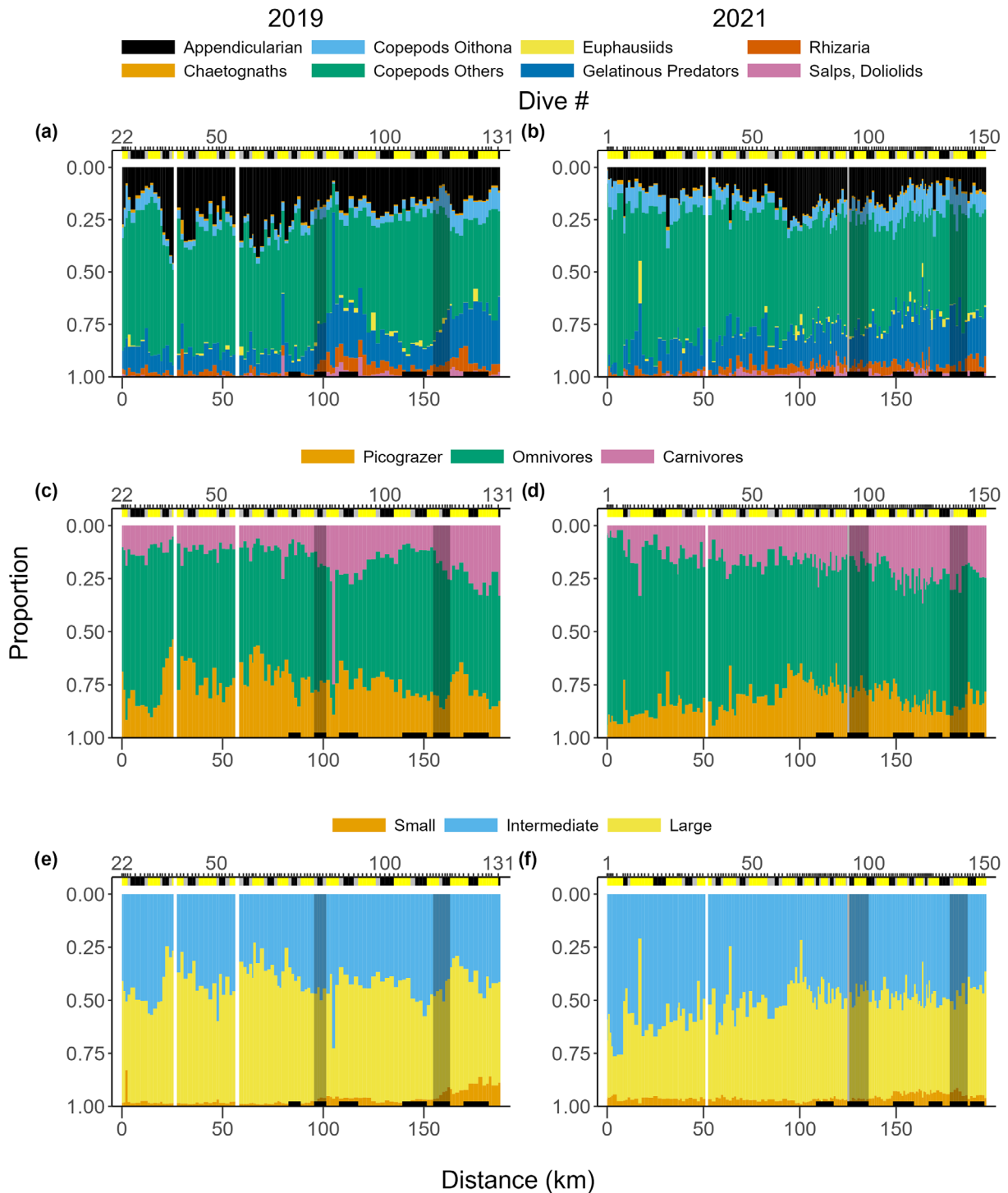


Fig. 8. Zooglider community structure based on proportional contribution to C biomass in the upper 100 m in (left column) 2019 and (right column) 2021. Top row (a, b): taxonomic composition. Middle row (c, d): dietary composition. Bottom row (e, f): size composition (small = 0.45–1 mm, intermediate = 1–3 mm, and large = > 3 mm). Other details as in Fig. 3.

contribution of appendicularians to particle export may be more significant inshore of the frontal features where their abundances are higher. In contrast, salps, whose tunics as well as rapidly sinking fecal pellets can dramatically increase particle

export to deep ocean waters (e.g., Henschke et al. 2013; Smith et al. 2014), may be more consequential to C export in the more offshore regions. The long-term benthic study site of Smith et al. (2014) at Station M, approximately 180 km from shore, appears

to be influenced by rapid vertical C export of such offshore salp populations.

The higher concentrations of marine snow in the inshore region also imply an enhanced contribution of snow-related particle export in the nearshore domain. While larger snow particles tend to sink faster than smaller ones, factors other than particle size, including variations in particle composition and ballasting minerals, also strongly influence particle export potential (Fender et al. 2019).

Copepods-other declined in concentration offshore of the California Current Front and decreased in average body size. This assemblage encompasses a heterogeneous group of copepods of diverse morphologies and phylogenetic affinities as well as different feeding behaviors (Mauchline 1998; Benedetti et al. 2016), Diel Vertical Migration responses (Ohman and Romagnan 2016), and other functional traits (Benedetti et al. 2016; Matthews and Blanco-Bercial 2023; Matthews and Ohman 2023). Hence, our aggregated category will certainly mask species-level differences in responses. However, this level of aggregation was necessitated by the efficacy of our current machine learning models, which perform much better for aggregated taxa. *Oithona*-like copepods are a sufficiently distinctive group optically for us to reliably differentiate them using our algorithms. They showed increased concentrations offshore in 2019 and midshore in 2021, in both cases suggesting that their prey fields, predator environment, and other aspects of their ocean habitat were less favorable in the nearshore environment of the California Current System. This distributional difference in relation to the other copepods sampled is consistent with the behavior of *Oithona* spp. as ambush predators and reliance on motile nanoplanktonic and microplanktonic prey (e.g., Drits and Semenova 1984; Uchima and Hirano 1986; Castellani et al. 2005). Such prey organisms, which are typically associated with the microbial food web, tend to predominate offshore of the major coastal upwelling environment in the California Current System (Kenitz et al. 2018; Taylor and Landry 2018). The enhanced abundances of *Oithona*-like copepods mid-to-offshore also imply a more favorable predation environment and reduced mortality rates (cf. Eiane and Ohman 2004). The overall decline in the proportional contribution of planktonic copepods in the offshore region, given their dominance in zooplankton biomass and importance as prey, predators, and vectors of carbon export, suggests a significant rearrangement of this component of the food web at these frontal gradients.

In terms of community structural changes, the most pronounced cross-shore shift was toward a higher proportion of carnivorous taxa in the offshore region, west of the inner front. This change was reflected in the higher proportions of cnidarians and ctenophores, plus chaetognaths, west (i.e., offshore) of the inner front. Although some representatives of other taxa (including copepods and euphausiids) can also be carnivorous, such distinctions could not be resolved here. A recent study involving DNA metabarcoding and trait-

based assignments across the California Current System similarly found a sharp decline in the proportions of herbivorous zooplankton taxa and increase in the relative importance of predatory taxa in the offshore California Current (Matthews and Ohman 2023).

As noted above, our analyses are limited by the taxonomic resolution that is currently achievable with in situ imaging and machine learning algorithms. For example, while our euphausiid category showed relatively little change across the major hydrographic gradients we have identified, it is well known that individual euphausiid species show clear hydrographic and biogeographic affinities in this region (e.g., Brinton et al. 1999; Lilly and Ohman 2021). Hence, we suspect that there were species-specific responses to these frontal features that are not resolved here. It is not feasible for us to resolve distributional changes associated with individual species as in Matthews and Ohman (2023). Nevertheless, the ability of *Zooglider* to resolve such gradients in near real-time, at high spatial resolution, and autonomously represents an advance over previous sampling approaches.

Does diel vertical migration behavior change across such frontal gradients?

The acoustic backscatter recorded by *Zooglider* is somewhat better suited to addressing the question of changes in Diel Vertical Migration (DVM) behavior because a much larger volume of water is sampled. Accordingly, at both 200 and 1000 kHz we detected a deepening of the daytime depth occupied by acoustic scattering layers as well as larger amplitude DVM in the offshore. These changes in habitat depth were closely associated with front-related changes in optical transparency, likely linked to light-mediated predation risk associated with attack by visually hunting predators. Light-mediated changes in habitat depths are well known for zooplankton in diverse aquatic environments (e.g., Buskey et al. 1989; Ringelberg 2010) as well as in this sector of the California Current System (Ohman and Romagnan 2016) and slightly further south (Gastauer et al. 2022). Such plasticity in habitat depth related to optical transparency is thought to be related to the elevated encounter distance with visually hunting predators in optically clearer waters, hence a need to seek a darker predation refuge in deeper depths.

In addition to DVM, the vertical habitats occupied by diverse organisms are consistent with other studies. Among the rhizarians we detected, the numerically dominant acantharians, which tend to bear photosymbionts, are often found in the euphotic zone (Biard and Ohman 2020). A similar pattern of vertical distribution has been found with collodarians in this region (Biard and Ohman 2020). Foraminifera tend to have a bimodal depth distribution, with some taxa residing in the euphotic zone and some in mesopelagic waters (Field 2004; Gaskell et al. 2019; Biard and Ohman 2020). Phaeodarians, as noted above, are most abundant below the euphotic zone (Biard and Ohman 2020). Among metazoans,

appendicularians tended to be distributed closer to the surface than planktonic copepods. This pattern was especially true in comparison with *Oithona*-like copepods that were rarely found near the sea surface and occupied deeper waters offshore of the California Current Front or the more inshore Front.

Are frontal regions sites of elevated biomass of phytoplankton, marine snow, or zooplankton?

Chl *a* fluorescence, as a proxy for phytoplankton biomass, was elevated only at the inshore front in 2019. There was no consistent evidence of enhanced (or reduced) volume backscatter (Sv) at frontal locations relative to the *Zooglider* dives immediately preceding and following. Although the median Sv at 200 and 1000 kHz was somewhat enhanced and the delta Sv was somewhat diminished (indicating a slight tendency toward greater contributions of larger backscatterers) at the California Current Front in both years, these changes were not statistically significant. This result contrasts with the findings of Powell and Ohman (2015b), who detected enhanced front-related Sv at 750 kHz when inshore waters were denser than offshore waters, and reduced front-related Sv when inshore waters were less dense than offshore waters. However, that study was based on a sample size of 81 front crossings, conferring considerably more statistical power than in the present crossings of 4 major fronts. The same authors found front-related enhancement in Chl *a* fluorescence when inshore waters were denser, and vice versa, again contrasting with most of the present results based on more limited frontal crossings. In all four of our fronts, inshore waters were denser than offshore waters.

Among zooplankton taxa there was no consistent indication of elevated (or reduced) abundances associated with all frontal crossings. However, copepods-other and acantharians were locally elevated at the inshore front in both years and appendicularians elevated at the inshore front in 2021. The pelagic tunicate group comprising salps + doliolids was locally depressed at the offshore front in both years. None of the carnivorous taxa showed front-related increases. These changes can be compared with the synthesis of Mangolte et al. (2023), who analyzed the extent of front-related enhancements of diverse planktonic taxa as sampled by nets and water bottles, across 10 frontal features, primarily in the more coastal part of our study region. The A-Front analyzed previously in this region is an example of a “peak” front with local aggregation of diverse organisms (Landry et al. 2012; Ohman et al. 2012). In their synthesis, Mangolte et al. found that diatoms and pico-grazers were elevated at 6 out of 10 fronts analyzed, including the A-Front. In general, “peak” fronts appear to be associated with more persistent hydrographic features, although the length of life of each feature is often difficult to assess (Mangolte et al. 2023). In the case of the fronts analyzed here, we do not have an estimate of the frontal persistence time. The California Current Front is likely to be relatively long-lived, as it is a major recurrent gradient region between the

inshore waters and offshore California Current. Notwithstanding this suspected longevity, the fronts we sampled appeared to be better characterized as “gradient” rather than “peak” frontal features. Even though a frontal feature itself may be persistent, the residence time of the fluid (and associated organisms) may be quite limited when currents are fast-flowing (Gangrade and Franks 2023), resulting in insufficient time for population growth of multicellular organisms to result in local accumulations.

Diverse responses to frontal features have been observed at different trophic levels and localities (e.g., Prants 2022). In the southern California Current System, the frontal boundaries of a recurrent eddy, sampled at relatively coarse (20 km) intervals, were not associated with pronounced changes in abundance of a suite of different copepods (Hauray 1984) or a cladoceran (Hauray et al. 1986) species. In high resolution sampling with a towed shadowgraph imaging system in the Southern California Bight, well south of our study region, most gelatinous taxa (pelagic tunicates, cnidarians, and ctenophores) were not concentrated at a sharp gradient region (Luo et al. 2014). However, of the 28 gelatinous taxa analyzed, 5 were found to be mildly or moderately aggregated, and 1 taxon (narcomedusae) highly aggregated at the frontal feature (Luo et al. 2014). From the same frontal study, but sampled with nets at much coarser horizontal spacing, none of 16 functional groups of zooplankton showed clear evidence of aggregation at the front (McClatchie et al. 2012), illustrating the importance of high spatial resolution sampling.

There were no consistent, localized front-associated increases (or decreases) in the concentration of marine snow, although there were abrupt declines in marine snow concentrations westward of the California Current front locations, as noted above.

Since frontal gradients are ubiquitous across diverse ocean environments ranging from coastal continental shelf regions to the open ocean, such features warrant additional attention in the future. With the advent of new high-resolution ocean altimetry (the SWOT satellite mission, Fu et al. 2024), the ability to remotely detect fine-scale ocean fronts has recently improved markedly. This capability, in turn, leads to a need for better approaches for resolving subsurface ecological and biogeochemical expressions of these fronts. The autonomous *Zooglider* is a particularly appropriate tool for resolving these gradients because of the nearly unprecedented fine-scale vertical resolution attainable with both optical imaging and dual-frequency acoustic sensors, extending to a depth of 400 m. Concurrent and continuous optical, acoustic, and physical measurements allow for direct analysis of biophysical coupling at a very fine scale. Summary data are telemetered in near-real time, permitting nearly instantaneous recognition of changing properties of the planktonic community and thus the ability to respond adaptively with either altered *Zooglider* trajectories or by guiding other sampling tools. Protracted missions at sea make it possible to sample diverse ocean features and to sense

organisms in a non-invasive manner in their natural habitat across multiple diel cycles.

Conclusions

Offshore of the California Current Front, in particular in the *Zooglider* study in 2019, we detected an abrupt decline in intensity of acoustic backscatter accompanied by a shift to smaller-bodied backscatterers. This change was associated with larger amplitude Diel Vertical Migrations to deeper daytime depths, in parallel with increased light transmission in overlying waters, apparently related to increased light-mediated predation risk. Zooplankton community composition and marine snow concentrations also changed across the frontal transitions. Gelatinous predators showed lower abundances in the inshore region, leading to an increase in the relative importance of carnivorous zooplankton in the offshore, with increased potential for top-down effects. These front-associated spatial community changes suggest larger potential contributions of marine snow, copepods, and appendicularians to export fluxes in the nearshore and enhanced contributions of salps and obligate predators to vertical fluxes in the offshore domain. There was partial evidence of enhanced local densities of organisms at the frontal gradients themselves, suggesting the fronts sampled were primarily transition gradients rather than sites of consistently elevated organismal abundances.

Data availability statement

The data that support the findings of this study are available from the corresponding author upon reasonable request.

References

- Allredge, A. L. 1972. Abandoned larvacean houses: A unique food source in the pelagic environment. *Science* **177**: 885–887. doi:10.1126/science.177.4052.885
- Belkin, I. M. 2021. Remote sensing of ocean fronts in marine ecology and fisheries. *Remote Sens. (Basel)* **13**: 883. doi:10.3390/rs13050883
- Belkin, I. M., P. C. Cornillon, and K. Sherman. 2009. Fronts in large marine ecosystems. *Prog. Oceanogr.* **81**: 223–236. doi:10.1016/j.pocean.2009.04.015
- Benedetti, F., S. Gasparini, and S. D. Ayata. 2016. Identifying copepod functional groups from species functional traits. *J. Plankton Res.* **38**: 159–166. doi:10.1093/plankt/fbv096
- Biard, T., and M. D. Ohman. 2020. Vertical niche definition of test-bearing protists (Rhizaria) into the twilight zone revealed by in situ imaging. *Limnol. Oceanogr.* **65**: 2583–2602. doi:10.1002/lno.11472
- Bone, Q. 1998. *The biology of pelagic tunicates*. Oxford Univ. Press.
- Brinton, E., M. D. Ohman, A. W. Townsend, M. D. Knight, and A. L. Bridgeman. 1999. *Euphausiids of the World Ocean*. UNESCO.
- Briseño-Avena, C., J. C. Prairie, P. J. S. Franks, and J. S. Jaffe. 2020. Comparing vertical distributions of Chl-a fluorescence, marine snow, and taxon-specific zooplankton in relation to density using high-resolution optical measurements. *Front. Mar. Sci.* **7**: 602. doi:10.3389/fmars.2020.00602
- Buskey, E. J., K. S. Baker, R. C. Smith, and E. Swift. 1989. Photosensitivity of the oceanic copepods *Pleuromamma gracilis* and *Pleuromamma xiphias* and its relationship to light penetration and daytime depth distribution. *Mar. Ecol. Prog. Ser.* **55**: 207–216. doi:10.3354/meps055207
- Castellani, C., X. Irigoien, R. P. Harris, and R. S. Lampitt. 2005. Feeding and egg production of *Oithona similis* in the North Atlantic. *Mar. Ecol. Prog. Ser.* **288**: 173–182. doi:10.3354/meps288173
- Chabert, P., F. d’ovidio, V. Echevin, M. R. Stukel, and M. D. Ohman. 2021. Cross-shore flow and implications for carbon export in the California Current Ecosystem: A Lagrangian analysis. *J. Geophys. Res. Oceans* **126**: e2020JC016611. doi:10.1029/2020JC016611
- Chavez, F. P., R. T. Barber, P. M. Kosro, A. Huyer, S. R. Ramp, T. P. Stanton, and B. Rojas de Mendiola. 1991. Horizontal transport and the distribution of nutrients in the coastal transition zone off northern California: Effects on primary production, phytoplankton biomass and species composition. *J. Geophys. Res. Oceans* **96**: 14833–14848.
- Chelton, D. B., M. G. Schlax, R. M. Samelson, and R. A. De Szoek. 2007. Global observations of large oceanic eddies. *Geophys. Res. Lett.* **34**: L15606. doi:10.1029/2007gl030812
- Dadon-Pilosof, A., F. Lombard, A. Genin, K. R. Sutherland, and G. Yahel. 2019. Prey taxonomy rather than size determines salp diets. *Limnol. Oceanogr.* **64**: 1996–2010. doi:10.1002/lno.11165
- Davis, C. S., S. M. Gallager, and A. R. Solow. 1992. Microaggregations of oceanic plankton observed by towed video microscopy. *Science* **257**: 230–232. doi:10.1126/science.257.5067.230
- De Robertis, A., and I. Higginbottom. 2007. A post-processing technique to estimate the signal-to-noise ratio and remove echosounder background noise. *ICES J. Mar. Sci.* **64**: 1282–1291. doi:10.1093/icesjms/fsm112
- De Robertis, A., D. R. McKelvey, and P. H. Ressler. 2010. Development and application of an empirical multifrequency method for backscatter classification. *Can. J. Fish. Aquat. Sci.* **67**: 1459–1474.
- Decima, M., M. R. Stukel, L. Lopez-Lopez, and M. R. Landry. 2019. The unique ecological role of pyrosomes in the Eastern Tropical Pacific. *Limnol. Oceanogr.* **64**: 728–743. doi:10.1002/lno.11071
- Deibel, D. 1998a. The abundance, distribution, and ecological impact of doliolids, p. 171–186. *In* Q. Bone [ed.], *The biology of pelagic tunicates*. Oxford Univ. Press.

- Deibel, D. 1998b. Feeding and metabolism of Appendicularia, p. 139–149. In Q. Bone [ed.], *The biology of pelagic tunicates*. Oxford Univ. Press.
- Demer, D. A., L. Berger, M. Bernasconi, E. Bethke, K. Boswell, D. Chu, R. Domokos, and others. 2015. Calibration of acoustic instruments, p. 133. ICES Cooperative Research Report No. 326.
- Drits, A. V., and T. N. Semenova. 1984. Experimental investigations of the feeding of *Oithona similis* Claus. *Oceanology* **24**: 755–759.
- Eiane, K., and M. D. Ohman. 2004. Stage specific mortality of *Calanus finmarchicus*, *Pseudocalanus elongatus* and *Oithona similis* on Fladen Ground, North Sea, during a spring bloom. *Mar. Ecol. Prog. Ser.* **268**: 183–193.
- Ellen, J. S., C. A. Graaf, and M. D. Ohman. 2019. Improving plankton image classification using context metadata. *Limnol. Oceanogr.: Methods* **17**: 439–461. doi:10.1002/lom3.10324
- Fakhraee, M., N. J. Planavsky, and C. T. Reinhard. 2020. The role of environmental factors in the long-term evolution of the marine biological pump. *Nat. Geosci.* **13**: 812–816.
- Fender, C. K., T. B. Kelly, L. Guidi, M. D. Ohman, M. C. Smith, and M. R. Stukel. 2019. Investigating particle size-flux relationships and the biological pump across a range of plankton ecosystem states from coastal to oligotrophic. *Front. Mar. Sci.* **6**: 603. doi:10.3389/fmars.2019.00603
- Fernandes, P. G., P. Stevenson, A. S. Brierley, F. Armstrong, and E. J. Simmonds. 2003. Autonomous underwater vehicles: Future platforms for fisheries acoustics. *ICES J. Mar. Sci.* **60**: 684–691. doi:10.1016/S1054-3139(03)00038-9
- Field, D. B. 2004. Variability in vertical distributions of planktonic foraminifera in the California Current: Relationships to vertical ocean structure. *Paleoceanography* **19**: PA2014. doi:10.1029/2003PA000970
- Francois, R. E., and G. R. Garrison. 1982a. Sound absorption based on ocean measurements: Part I: Pure water and magnesium sulfate contributions. *J. Acoust. Soc. Am.* **72**: 896–907. doi:10.1121/1.388170
- Francois, R. E., and G. R. Garrison. 1982b. Sound absorption based on ocean measurements. Part II: Boric acid contribution and equation for total absorption. *J. Acoust. Soc. Am.* **72**: 1879–1890. doi:10.1121/1.388673
- Fu, L.-L., and others. 2024. The surface water and ocean topography mission: A breakthrough in radar remote sensing of the ocean and land surface water. *Geophys. Res. Lett.* **51**: e2023GL107652. doi:10.1029/2023gl107652
- Gangrade, S., and P. J. S. Franks. 2023. Phytoplankton patches at oceanic fronts are linked to coastal upwelling pulses: Observations and implications in the California Current System. *J. Geophys. Res. Oceans* **128**: e2022JC019095. doi:10.1029/2022jc019095
- Gaskell, D. E., M. D. Ohman, and P. M. Hull. 2019. *Zooglider*-based measurements of planktonic foraminifera in the California Current System. *J. Foraminifer. Res.* **49**: 390–404. doi:10.2113/gsjfr.49.4.390
- Gastauer, S., C. F. Nickels, and M. D. Ohman. 2022. Body size- and season-dependent diel vertical migration of mesozooplankton resolved acoustically in the San Diego Trough. *Limnol. Oceanogr.* **67**: 300–313. doi:10.1002/lno.11993
- Greenlaw, C. F. 1979. Acoustical estimation of zooplankton populations. *Limnol. Oceanogr.* **24**: 226–242. doi:10.4319/lo.1979.24.2.0226
- Haëck, C., M. Lévy, I. Mangolte, and L. Bopp. 2023. Satellite data reveal earlier and stronger phytoplankton blooms over fronts in the Gulf Stream region. *Biogeosciences* **20**: 1741–1758. doi:10.5194/bg-20-1741-2023
- Haury, L. R. 1984. An offshore eddy in the California Current System. Part IV: Plankton distributions. *Prog. Oceanogr.* **13**: 95–111. doi:10.1016/0079-6611(84)90007-7
- Haury, L. R., J. J. Simpson, J. Peláez, C. J. Koblinsky, and D. Wiesenhahn. 1986. Biological consequences of a recurrent eddy off point conception, California. *J. Geophys. Res. Oceans* **91**: 12937–12956.
- Henschke, N., and others. 2013. Salp-falls in the Tasman Sea: A major food input to deep-sea benthos. *Mar. Ecol. Prog. Ser.* **491**: 165–175. doi:10.3354/meps10450
- Hickey, B. M. 1979. The California Current System—Hypotheses and facts. *Prog. Oceanogr.* **8**: 191–279.
- Kahru, M., M. G. Jacox, and M. D. Ohman. 2018. CCE1: Decrease in the frequency of oceanic fronts and surface chlorophyll concentration in the California Current System during the 2014–2016 northeast Pacific warm anomalies. *Deep-Sea Res. I Oceanogr. Res. Pap.* **140**: 4–13. doi:10.1016/j.dsr.2018.04.007
- Keates, T. R., and others. 2022. Foraging behavior of a mesopelagic predator, the northern elephant seal, in northeastern Pacific eddies. *Deep-Sea Res. I-Oceanogr. Res. Pap.* **189**: 103866. doi:10.1016/j.dsr.2022.103866
- Kenitz, K. M., A. Visser, M. D. Ohman, M. D. Landry, and K. H. Andersen. 2018. Community trait distribution across environmental gradients. *Ecosystems* **22**: 968–980. doi:10.1007/s10021-018-0314-5
- Korneliussen, R. J. [ed.]. 2018. Acoustic target classification, p. 104. ICES Cooperative Research Report No. 344. doi:10.17895/ices.pub.4567
- Landry, M. R., and others. 2012. Pelagic community responses to a deep-water front in the California Current Ecosystem: Overview of the A-Front Study. *J. Plankton Res.* **34**: 739–748. doi:10.1093/plankt/fbs025
- Lavaniegos, B. E., and M. D. Ohman. 2007. Coherence of long-term variations of zooplankton in two sectors of the California Current System. *Prog. Oceanogr.* **75**: 42–69. doi:10.1016/j.pocean.2007.07.002
- Lévy, M., P. J. S. Franks, and K. S. Smith. 2018. The role of submesoscale currents in structuring marine ecosystems. *Nat. Commun.* **9**: 4758. doi:10.1038/s41467-018-07059-3
- Li, Q. P., P. J. S. Franks, and M. R. Landry. 2017. Recovering growth and grazing rates from nonlinear dilution experiments. *Limnol. Oceanogr.* **62**: 1825–1835. doi:10.1002/lno.10536

- Lilly, L. E., and M. D. Ohman. 2021. Euphausiid spatial displacements and habitat shifts in the southern California Current System in response to El Niño variability. *Prog. Oceanogr.* **193**: 102544. doi:[10.1016/j.pocean.2021.102544](https://doi.org/10.1016/j.pocean.2021.102544)
- Luo, J. Y., and others. 2014. Environmental drivers of the fine-scale distribution of a gelatinous zooplankton community across a mesoscale front. *Mar. Ecol. Prog. Ser.* **510**: 129–149. doi:[10.3354/meps10908](https://doi.org/10.3354/meps10908)
- Lynn, R. J., and J. J. Simpson. 1987. The California Current System: The seasonal variability of its physical characteristics. *J. Geophys. Res.* **92**: 12947–12966. doi:[10.1029/JC092iC12p12947](https://doi.org/10.1029/JC092iC12p12947)
- Macaulay, G. J., D. Z. Chu, and E. Ona. 2020. Field measurements of acoustic absorption in seawater from 38 to 360 kHz. *J. Acoust. Soc. Am.* **148**: 100–107. doi:[10.1121/10.0001498](https://doi.org/10.1121/10.0001498)
- Mackenzie, K. V. 1981. Nine-term equation for sound speed in the oceans. *J. Acoust. Soc. Am.* **70**: 807–812. doi:[10.1121/1.386920](https://doi.org/10.1121/1.386920)
- Mangolte, I., M. Lévy, S. Dutkiewicz, S. Clayton, and O. Jahn. 2022. Plankton community response to fronts: Winners and losers. *J. Plankton Res.* **44**: 241–258. doi:[10.1093/plankt/fbac010](https://doi.org/10.1093/plankt/fbac010)
- Mangolte, I., M. Lévy, C. Haëck, and M. D. Ohman. 2023. Sub-frontal niches of plankton communities driven by transport and trophic interactions at ocean fronts. *Biogeosciences* **20**: 3273–3299. doi:[10.5194/bg-20-3273-2023](https://doi.org/10.5194/bg-20-3273-2023)
- Matthews, S. A., and L. Blanco-Bercial. 2023. Divergent patterns of zooplankton connectivity in the epipelagic and mesopelagic zones of the eastern North Pacific. *Ecol. Evol.* **13**: e10664. doi:[10.1002/ece3.10664](https://doi.org/10.1002/ece3.10664)
- Matthews, S. A., and M. D. Ohman. 2023. A space-for-time framework for forecasting the effects of ocean stratification on zooplankton vertical habitat use and trait composition. *Limnol. Oceanogr.* **68**: 2688–2702. doi:[10.1002/lno.12450](https://doi.org/10.1002/lno.12450)
- Mauchline, J. 1998. The biology of calanoid copepods. *Adv. Mar. Biol.* **33**: 1–701.
- McClatchie, S., and others. 2012. Resolution of fine biological structure including small narcomedusae across a front in the Southern California Bight. *J. Geophys. Res. Oceans* **117**: C04020. doi:[10.1029/2011JC007565](https://doi.org/10.1029/2011JC007565)
- McDougall, T. J., and O. A. Krzysik. 2015. Spiciness. *J. Mar. Res.* **73**: 141–152.
- Mignot, A., R. Ferrari, and H. Claustre. 2018. Floats with bio-optical sensors reveal what processes trigger the North Atlantic bloom. *Nat. Commun.* **9**: 190. doi:[10.1038/s41467-017-02143-6](https://doi.org/10.1038/s41467-017-02143-6)
- Ohman, M. D., J. R. Powell, M. Picheral, and D. W. Jensen. 2012. Mesozooplankton and particulate matter responses to a deep-water frontal system in the southern California Current System. *J. Plankton Res.* **34**: 815–827. doi:[10.1093/plankt/fbs028](https://doi.org/10.1093/plankt/fbs028)
- Ohman, M. D., and J. B. Romagnan. 2016. Nonlinear effects of body size and optical attenuation on Diel Vertical Migration by zooplankton. *Limnol. Oceanogr.* **61**: 765–770. doi:[10.1002/lno.10251](https://doi.org/10.1002/lno.10251)
- Ohman, M. D., R. E. Davis, J. T. Sherman, K. R. Grindley, B. M. Whitmore, C. F. Nickels, and J. S. Ellen. 2018. *Zoo-glider*: An autonomous vehicle for optical and acoustic sensing of zooplankton. *Limnol. Oceanogr.: Methods* **17**: 69–86. doi:[10.1002/lom3.10301](https://doi.org/10.1002/lom3.10301)
- Picheral, M., and others. 2022. The Underwater Vision Profiler 6: An imaging sensor of particle size spectra and plankton, for autonomous and cabled platforms. *Limnol. Oceanogr.: Methods* **20**: 115–129. doi:[10.1002/lom3.10475](https://doi.org/10.1002/lom3.10475)
- Powell, J. R., and M. D. Ohman. 2015a. Covariability of zooplankton gradients with glider-detected density fronts in the Southern California Current System. *Deep-Sea Res. II Top. Stud. Oceanogr.* **112**: 79–90. doi:[10.1016/j.dsr2.2014.04.002](https://doi.org/10.1016/j.dsr2.2014.04.002)
- Powell, J. R., and M. D. Ohman. 2015b. Changes in zooplankton habitat, behavior, and acoustic scattering characteristics across glider-resolved fronts in the Southern California Current System. *Prog. Oceanogr.* **134**: 77–92. doi:[10.1016/j.pocean.2014.12.011](https://doi.org/10.1016/j.pocean.2014.12.011)
- Prants, S. V. 2022. Marine life at Lagrangian fronts. *Prog. Oceanogr.* **204**: 102790. doi:[10.1016/j.pocean.2022.102790](https://doi.org/10.1016/j.pocean.2022.102790)
- Ringelberg, J. 2010. Diel vertical migration of zooplankton in lakes and oceans: Causal explanations and adaptive significances. Springer Press.
- Robison, B. H., K. R. Reisenbichler, and R. E. Sherlock. 2005. Giant larvacean houses: Rapid carbon transport to the deep sea floor. *Science* **308**: 1609–1611. doi:[10.1126/science.1109104](https://doi.org/10.1126/science.1109104)
- Schmid, M. S., R. K. Cowen, K. Robinson, J. Y. Luo, C. Briseno-Avena, and S. Sponaugle. 2020. Prey and predator overlap at the edge of a mesoscale eddy: Fine-scale, in-situ distributions to inform our understanding of oceanographic processes. *Sci. Rep.* **10**: 921. doi:[10.1038/s41598-020-57879-x](https://doi.org/10.1038/s41598-020-57879-x)
- Smith, J., and others. 2014. Large salp bloom export from the upper ocean and benthic community response in the abyssal northeast Pacific: Day to week resolution. *Limnol. Oceanogr.* **59**: 745–757. doi:[10.4319/lo.2014.59.3.0745](https://doi.org/10.4319/lo.2014.59.3.0745)
- Stanton, T. K., D. Chu, and P. H. Wiebe. 1996. Acoustic scattering characteristics of several zooplankton groups. *ICES J. Mar. Sci.* **53**: 289–295.
- Stukel, M. R., and others. 2017. Mesoscale ocean fronts enhance carbon export due to gravitational sinking and subduction. *Proc. Nat. Acad. Sci. USA* **114**: 1252–1257. doi:[10.1073/pnas.1609435114](https://doi.org/10.1073/pnas.1609435114)
- Sutherland, K. R., L. P. Madin, and R. Stocker. 2010. Filtration of submicrometer particles by pelagic tunicates. *Proc. Natl. Acad. Sci. USA* **107**: 15129–15134. doi:[10.1073/pnas.1003599107](https://doi.org/10.1073/pnas.1003599107)

- Taylor, A. G., and M. R. Landry. 2018. Phytoplankton biomass and size structure across trophic gradients in the southern California Current and adjacent ocean ecosystems. *Mar. Ecol. Prog. Ser.* **592**: 1–17. doi:[10.3354/meps12526](https://doi.org/10.3354/meps12526)
- Uchima, U., and R. Hirano. 1986. Food of *Oithona davisae* (Copepoda: Cyclopoida) and the effect of food concentration at first feeding on the larval growth. *Bull. Plankton Soc. Japan* **33**: 21–28.
- Whitmore, B. M., and M. D. Ohman. 2021. *Zooglider*-measured association of zooplankton with the fine scale vertical prey field. *Limnol. Oceanogr.* **66**: 3811–3827. doi:[10.1002/lno.11920](https://doi.org/10.1002/lno.11920)
- Wiebe, P. H., and M. C. Benfield. 2003. From the Hensen net toward four-dimensional biological oceanography. *Prog. Oceanogr.* **56**: 7–136. doi:[10.1016/S0079-6611\(02\)00140-4](https://doi.org/10.1016/S0079-6611(02)00140-4)
- Yamahara, K. M., and others. 2019. *In situ* autonomous acquisition and preservation of marine environmental DNA using an autonomous underwater vehicle. *Front. Mar. Sci.* **6**: 373. doi:[10.3389/fmars.2019.00373](https://doi.org/10.3389/fmars.2019.00373)

Acknowledgments

S. Gastauer and M.D. Ohman received financial support from the Gordon and Betty Moore Foundation. Also supported by NSF via the California Current Ecosystem Long-Term Ecological Research site. We express thanks to the Scripps Instrument Development Group for the development and support of *Zooglider*, Jeffrey S. Ellen for machine learning classifications of the Zoocam images, and Mati Kahru for providing processed satellite data. The LOCEAN group at Sorbonne University, Paris, kindly provided facilities during manuscript preparation. Open Access funding enabled and organized by Projekt DEAL.

Conflict of Interest

None declared.

Submitted 20 February 2024

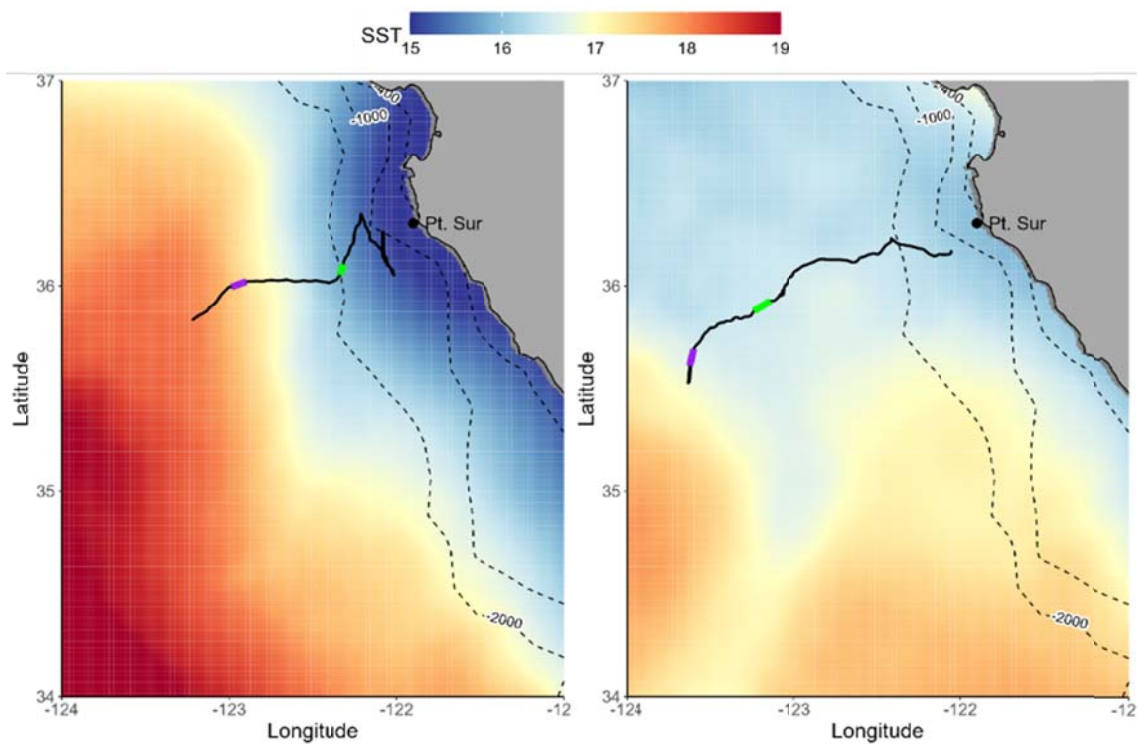
Revised 26 June 2024

Accepted 09 July 2024

Associate editor: Yui Takeshita

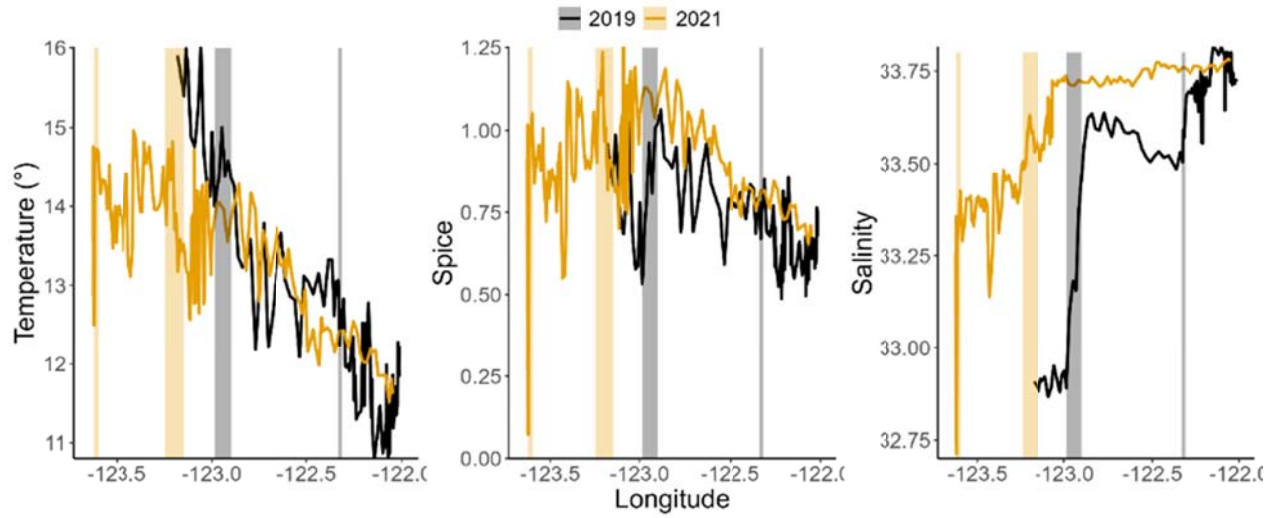
1 **Supplementary material**

2



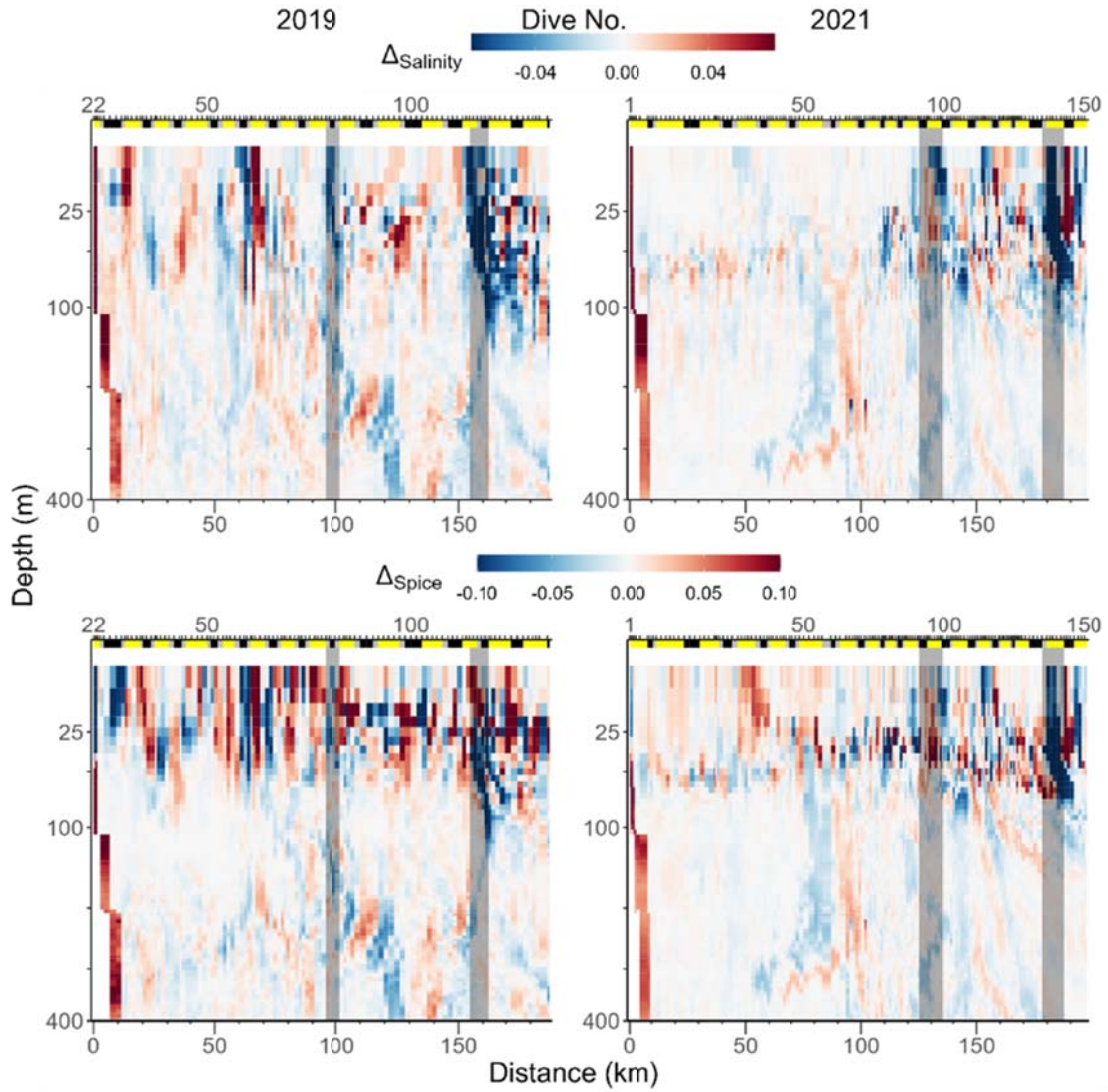
3

4 **Fig. S1.** *Zooglider* mission paths in 2019 (left) and 2021 (right), with an indication of the
5 inshore (green bar) and offshore (magenta bar) frontal locations. The mission paths are plotted on
6 the averaged sea surface temperature values derived from the NASA daily Multi-scale Ultra-high
7 Resolution (MUR) Sea Surface Temperature (SST) Analysis over the time period of *Zooglider*
8 missions. Dashed contours show depth in m.



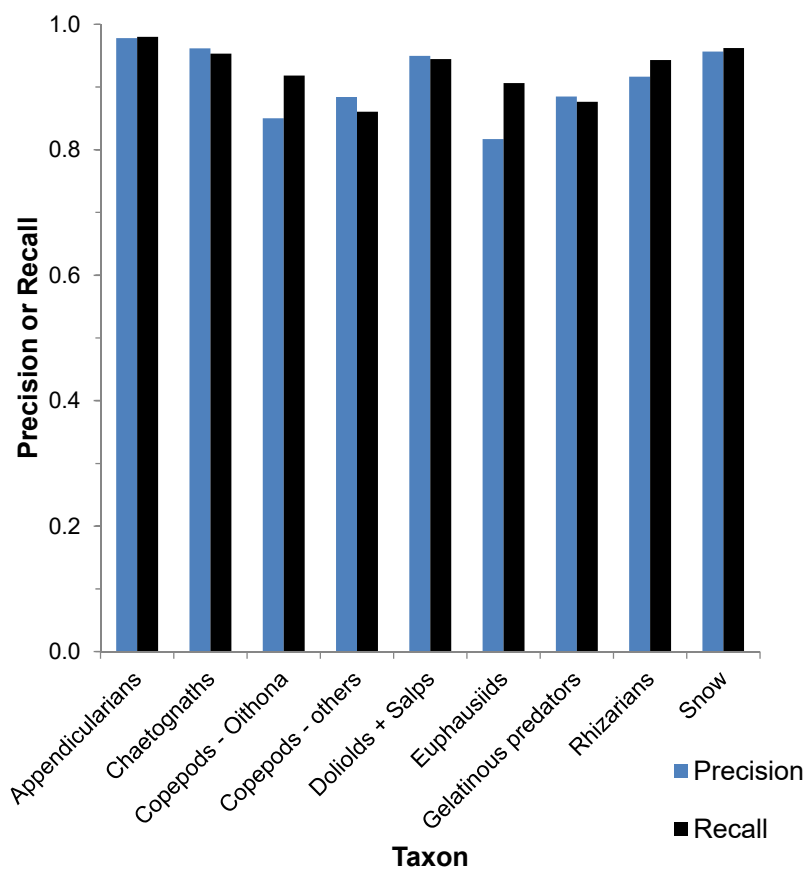
9

10 **Fig. S2.** Along-glider track average salinity, spiciness, and temperature for the upper 50 m of
 11 the 2019 and 2021 missions for each dive. Inshore is to the right and offshore (west) to the left.
 12 Frontal regions are indicated by shaded rectangles.



13

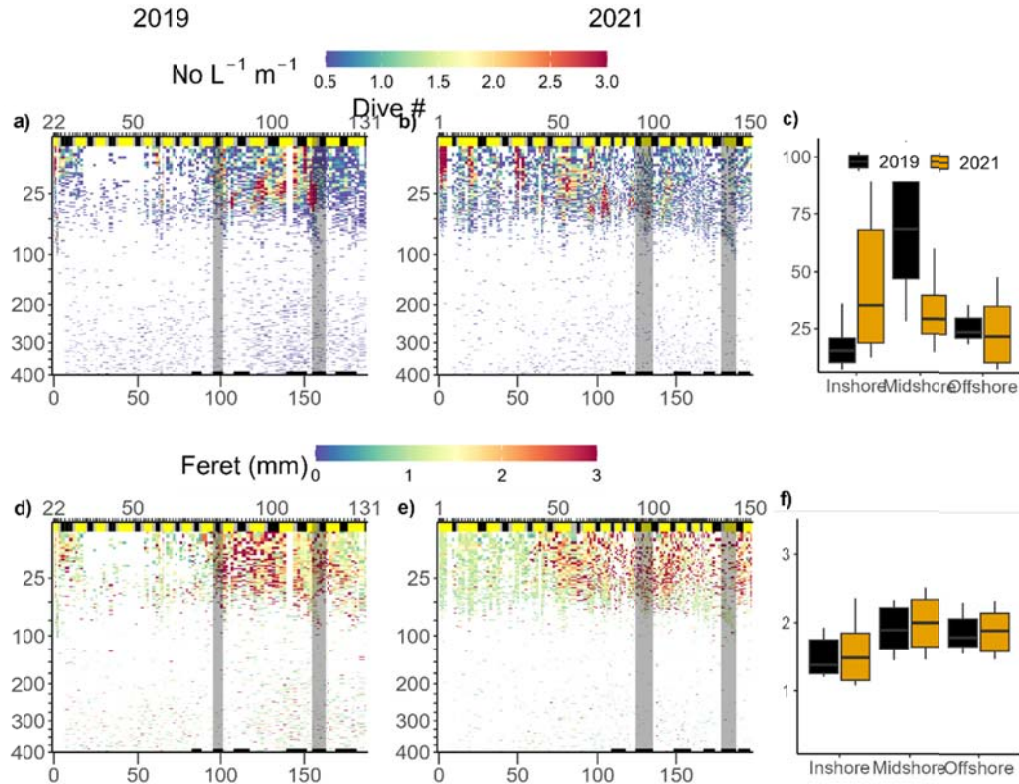
14 **Fig. S3.** *Zooglider* sections of the horizontal gradients of (top row) salinity and (bottom row)
 15 spiciness. Two major frontal regions are indicated by vertical grey bars in both (left column)
 16 2019 and (right column) 2021. Other details as in Fig. 1.



17

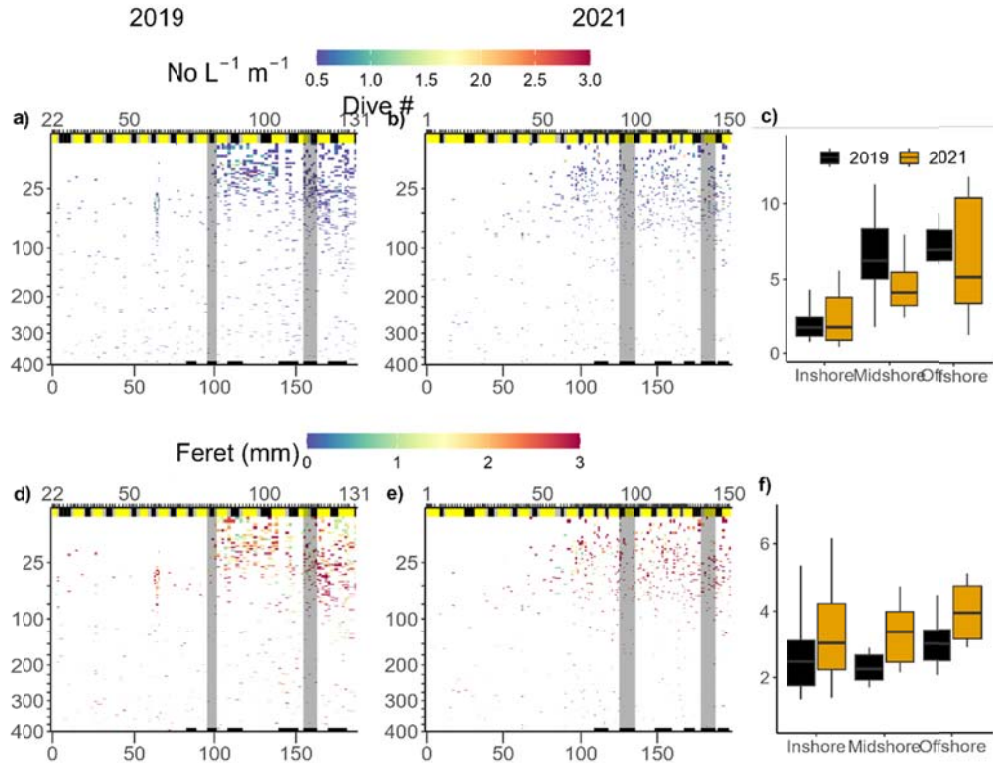
18 **Fig. S4.** Machine Learning Precision and Recall for the major taxa analyzed in this

19 study.



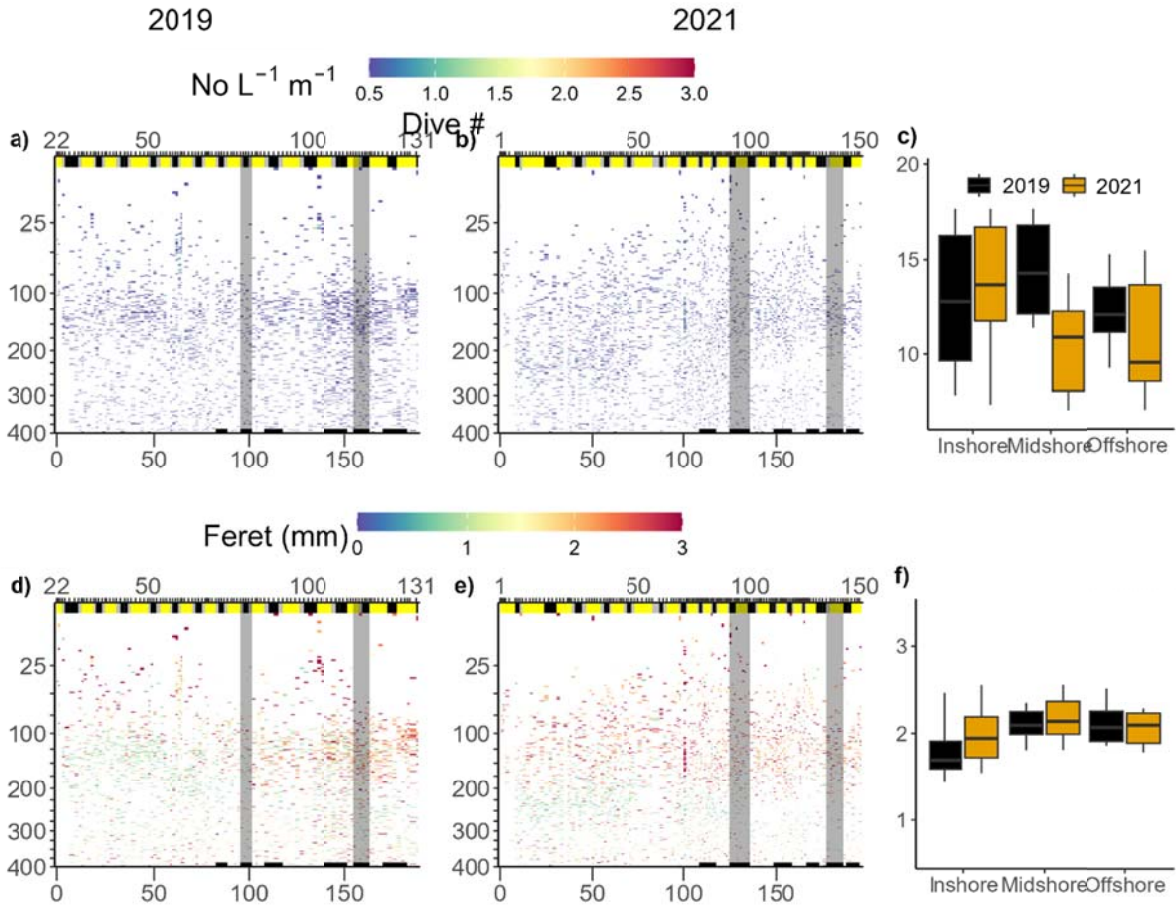
20

21 **Fig. S5.** Acantharians. Upper row: concentration (a-b, No. L⁻¹) and Lower row: size (d-e, feret
 22 diameter, mm). *Zooglider* deployments in (left columns) 2019 and (center columns) 2021. Top
 23 color bar indicates day (yellow), dusk/dawn (grey) or night (black) dives. Horizontal black bars at
 24 the bottom of each figures indicate locations of dives preceding, inside, and following the peak
 25 frontal gradients. Vertical grey bars indicate the locations of the inshore front (left bar in both
 26 panels) and offshore front (right bar in both panels). Top x-axis indicates dive number, bottom x-
 27 axis indicates distance travelled (km). Note that the z-axis has been square root-transformed.
 28 Boxplots in right columns grouped by year (black = 2019, orange = 2021) and by region inshore
 29 of the inner front, midshore between the two fronts, or offshore (west) of the front. Box plots
 30 indicate median \pm 10th and 90th percentiles.



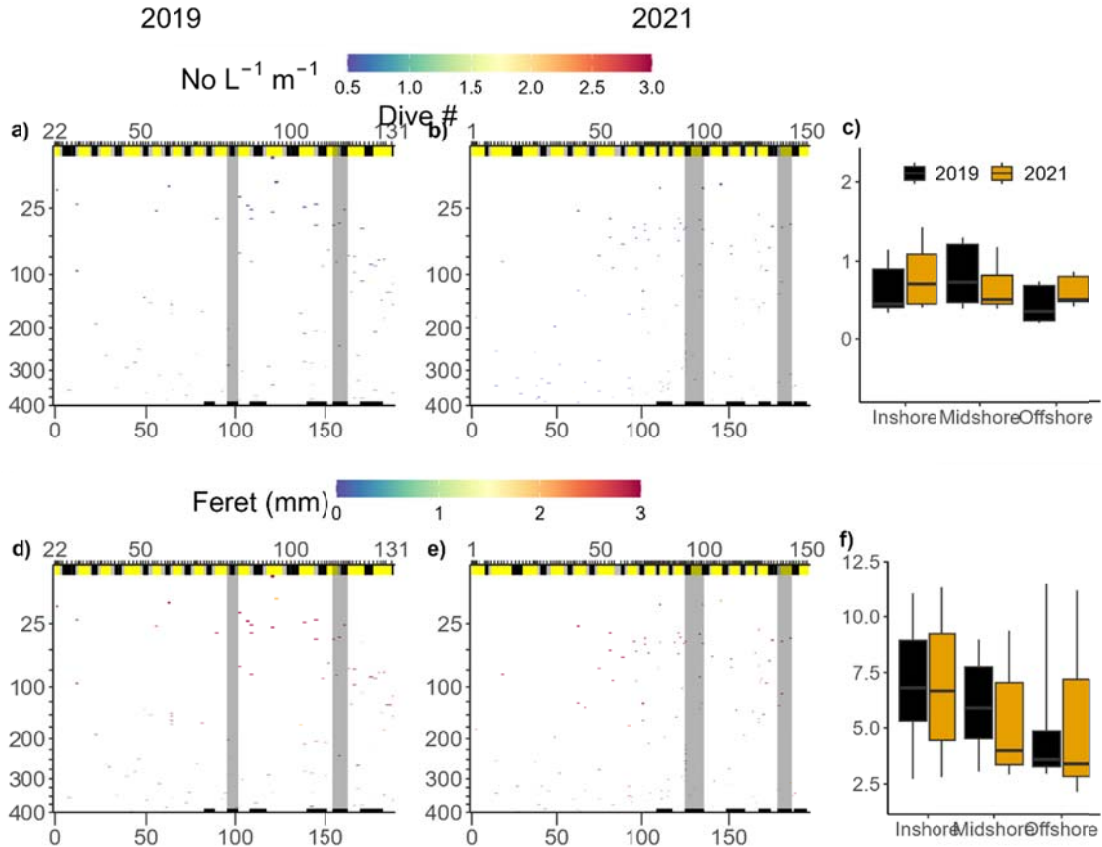
31

32 **Fig. S6.** Collodarians. Upper row: concentration (a-b, No. L⁻¹) and Lower row: size (d-
 33 e, feret diameter, mm). *Zooglider* deployments in (left columns) 2019 and (center columns)
 34 2021. Boxplots in right columns grouped by year (black = 2019, orange = 2021) and by region
 35 inshore of the inner front, midshore between the two fronts, or offshore (west) of the front. Other
 36 details as in Fig. S5.



37

38 **Fig. S7.** Phaeodarians. Upper row: concentration (a-b, No. L^{-1}) and Lower row: size (d-e,
 39 feret diameter, mm). *Zooglider* deployments in (left columns) 2019 and (center columns) 2021.
 40 Boxplots in right columns grouped by year (black = 2019, orange = 2021) and by region inshore
 41 of the inner front, midshore between the two fronts, or offshore (west) of the front. Other details
 42 as in Fig. S5.



43

44 **Fig. S8.** Foraminifera. Upper row: concentration (a-b, No. L⁻¹) and Lower row: size (d-e,

45 feret diameter, mm). *Zooglider* deployments in (left columns) 2019 and (center columns) 2021.

46 Boxplots in right columns grouped by year (black = 2019, orange = 2021) and by region inshore

47 of the inner front, midshore between the two fronts, or offshore (west) of the front. Other details

48 as in Fig. S5.

49 **Table S1.** Mean and 95% confidence intervals for Temperature, Salinity, and Spiciness for the
 50 upper 100 m. Sample size (N) indicated in the rightmost column.

		Temperature	Salinity	Spice	N
2019	Inshore	10.77 (± 0.06)	33.80 ($\pm < 0.01$)	0.53 (± 0.01)	1867
	Midshore	11.52 (± 0.14)	33.67 (± 0.01)	0.60 (± 0.02)	882
	Offshore	12.78 (± 0.25)	33.14 (± 0.03)	0.47 (± 0.05)	541
2021	Inshore	11.59 (± 0.07)	33.77 ($\pm < 0.01$)	0.68 (± 0.01)	2847
	Midshore	12.25 (± 0.10)	33.48 (± 0.01)	0.60 (± 0.02)	1588
	Offshore	12.41 (± 0.18)	33.12 (± 0.03)	0.36 (± 0.04)	395

52 **Table S2.** Relationship between carbon content (C, μgC) and feret diameter (fd, mm), modified
 53 from Lavaniegos and Ohman (2007) for Zoocam measurements.

Taxonomic Group	Feret Diameter to C
Appendicularians	$C = 0.49 (38.8 (0.262 \text{ fd})^{2.574})^{1.12}$
Chaetognaths	$C = 0.0956 (1.04 \text{ fd})^{2.9093}$
Copepods (calanoid)	$C = 10^{-6.76 + 2.512 \log (690 \text{ fd})}$
Copepods (<i>Oithona</i>)	$C = 10^{-6.76 + 2.512 \log (640 \text{ fd})}$
Copepods (mean calanoid and <i>Oithona</i>)	$C = 10^{-6.76 + 2.512 \log (670 \text{ fd})}$
Ctenophores	$C = 4.8 (0.921 \text{ fd})^{1.775}$
Euphausiids	$C = 10^{-0.473 + 3.174 \log_{10}(1.04 \text{ fd})}$
Medusae	$C = 1.8885 (0.799 \text{ fd})^{2.3619}$
Salps	$C = 1.49 (1.001 \text{ fd})^{2.00}$
Doliolids	$C = 0.51 (0.963 \text{ fd})^{2.28}$
Doliolids / Salps	$C = (1.49 (1.001 \text{ fd})^{2.00} + 0.51 (0.963 \text{ fd})^{2.28})/2$

55 **Table S3.** Spearman's rank correlation coefficients between K_{d490} and daytime depths of volume
56 backscatter (S_v) at 200 and 1000 kHz, in 2019 and 2021.

Year	Frequency (kHz)	Test Statistic (S)	rho	p
2019	200	852.3	-0.873	<0.001
2021	200	824.22	-0.812	<0.001
2019	1000	1107.6	-0.629	0.009
2021	1000	1008.0	-0.482	0.06

57

58